Energy Equip. Sys./ Vol. 11/No. 3/September 2023/ 277-304

ENERGY EQUIPSYS

Energy Equipment and Systems
http://energyequipsys.ut.ac.ir
www.energyequipsys.com

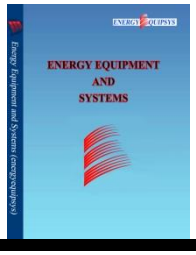

Thermodynamic analysis of sustainable electric power production using solar towers during the day and syngas combustion from municipal waste gasification during the night

Authors

Mohsen Zeinali[a]*
Ali Sharifi[a]
Faramarz Ranjbar[a]

[a]Department of Mechanical Engineering, Faculty of Mechanical Engineering, University of Tabriz, Tabriz, Iran

Article history:

Received : 30 March 2023

Accepted : 14 May 2023

ABSTRACT

Solar power plants have received much attention in recent years due to the use of renewable energy sources, no production of polluting gases, high concentration ratio, and proper thermal efficiency. But solar radiation's absence at night prevents the uniform and continuous production of electricity. Also, the challenge of the ever-increasing accumulation of municipal waste has caused the waste fuel-based power plants to attract the attention of many industrialized and developing countries. In the present research, a practical solution is proposed to solve the challenge of not producing electricity in solar tower power plants during the night by using waste as the input fuel of the power plant. The results obtained from the case study of the investigated cogeneration system show that the electric powers produced by the subsystems of the air Brayton cycle, the reheat Rankine cycle, and the organic Rankine cycle are equal to 4502.6 KW, 2640.3 KW, and 118 KW, respectively. The central receiver of the solar tower has the highest rate of irreversibility, accounting for 34% of the total exergy destruction rate. Based on the parametric study results, the irreversibility of the entire cogeneration system has a direct relationship with the inlet temperature of the turbine. Increasing the moisture of the waste also leads to a decrease in the temperature and percentage of syngas produced, and causes a decrease in the overall performance of the system. The net power of the cogeneration system increases first and then decreases with the increase in the temperature of the gasification process.

Keywords: Sustainable Energy System; Solar Tower; Gasification; Thermodynamic Analysis; Cogeneration System.

1. Introduction

According to the world population growth, it is estimated that the population will increase by 30% in the next 50 years [1]. Human life depends on the use of energy, which is constantly growing. In the last few decades, due to technological advancements and the increase in the social welfare level, many countries have reached a steep slope in

* Corresponding author: Mohsen Zeinali
Department of Mechanical Engineering, Faculty of Mechanical Engineering, University of Tabriz, Tabriz, Iran
Email: mohsenzeinali98@ms.tabrizu.ac.ir

increasing the utilization of fossil fuels. This has brought many negative consequences such as climate change, environmental pollution, reduction of natural resource reserves, etc. [2]. Among the most important challenges today are energy, the environment, and the economy. The relationship between these three parameters is very important and complex and depends on government policies.

Fossil fuel sources utilization has two important problems: first, their resources have limited capacities and are exhaustible; Secondly, these sources release abundant gaseous and liquid pollutants [3]. For this purpose, renewable energies have been considered as suitable alternatives to fossil fuels in recent years. Among renewable energies, solar energy is an inexhaustible, available, clean, safe, and secure source, and it will definitely be one of the most promising and sustainable options for electricity generation in the future [4]. The radiant energy of the sun that reaches the earth's surface in one hour is equivalent to one year's energy consumption of the entire planet [2]. Generally, the applications of solar energy can be classified into two categories: power plant applications and non-power plant applications. Non-power plant applications include solar heating and cooling, solar water heaters, solar water desalination units, solar dryers, solar furnaces, medical uses, and solar houses; However, the most important application of solar energy, which is also the subject of the present research, includes power plant applications and electric power generation from solar energy. The intensity of solar radiation varies throughout the day. The production of solar electricity is limited during peak times when the price of electricity increases. The reliability of solar power plants highly depends on the level of technologies used (such as the type of solar cells chosen for the photovoltaic power plant); Also, controlling and managing the solar power plant is one of the other challenges. There are two general solutions to reduce these challenges: The first solution is to link the solar power plant with a backup system, such as a system based on fossil fuels or a system based on other renewable energy sources like biomass fuel. The backup system compensates for natural changes in the intensity of solar radiation and makes it possible to produce electricity when it is absent or reduced. The second solution is to combine the energy storage technologies with the solar power plant. Combining the energy storage system with solar concentrator generators will increase operating hours and compensate for short-term fluctuations. Several types of thermal energy storage for solar power plants have been made of the type of parabolic mirrors and central receivers with the possibility of generating electricity for 12 hours [2]. In the present research, we will focus on the use of hybrid-solar and backup systems to achieve the goal of uniform and sustainable production of electric power throughout the day.

Central receiver type (CRS) solar power plants, which are also called solar towers, are one of the most important types of solar power plants that have received much attention due to their high operating temperatures and thermal efficiency. Also, it is possible to build these power plants on very large scales [5]. The solar tower was first proposed by Russian scientists in the mid-1950s, and various experiments on central receivers were first carried out in 1960 at the University of Genoa, Italy, by Professor Giovani; However, the technology of central receivers has been the focus of many countries since the early 1980s [6]. The solar tower system consists of a field of mirrors (which are also called heliostats) that can rotate along two axes. These mirrors reflect sunlight back to a receiver located on top of the central tower. In order to increase the operating time of the power plant and generate stable electricity even when there is no sunlight, it is possible to use the storage system or the backup system for the hybrid operation of the power plant [7].

Tukenmez et al. [8] performed a parametric analysis of a multi-generation power plant based on solar energy combined with a gas turbine to produce hydrogen. This power plant consisted of sub-systems of supercritical carbon dioxide, ejector refrigeration, organic Rankine, solar tower, hydrogen production and liquefaction, and water heater. The solar power plant subsystem provided the required energy for air, water, and fuel preheaters in the solid oxide fuel cell subsystem. Also, the afterburner exhaust gases were used in the supercritical carbon dioxide cycle's heat exchangers, organic Rankine cycle's generator, water preheater,

proton exchange fuel cell, and hot water generator, respectively. By adding a gas turbine sub-system, electric powers of 6482 KW and 7053 KW were produced, respectively. Also, in the combined plant, the exergy efficiency of hydrogen production and liquefaction reached 48.53%. The hydrogen production rate was also calculated as 0.0642 kg/s.

Dunham and Iverson [9] evaluated the utilization of solar concentrator systems in different thermodynamic cycles. The investigated systems include Brayton helium cycle, Brayton carbon dioxide cycle with a regenerator, steam Rankine cycle, combined CO_2-ORC cycle, and recompression Brayton CO_2 cycle. In each of the proposed cases, system efficiency was evaluated at different temperature conditions. They concluded that with the limitations related to the materials of the steam cycle equipment, the cycle operated at high efficiency with the temperature being at the maximum value of 600°C and for the temperatures higher than that, the recompression Brayton CO_2 cycle had better thermal performance. Cen et al. [10] proposed a new power generation system based on gas turbine and solar energy and analyzed it from exergy, economic, and environmental perspectives. In their proposed system, ambient air, after passing through the photovoltaic panel and receiving heat, entered the gasification system and after combining it with biomass fuel, syngas were produced. After generating power in the high-pressure turbine, the hot gases from biomass combustion flowed to the hydrogen combustion chamber and by injecting fuel, the chamber reheated the syngas. The hydrogen fuel required for the combustion chamber was produced in an electrolysis unit and the electric power needed for the process was provided by photovoltaic panels. The results of the study revealed that among the components of the proposed system, the photovoltaic panel and the air compressor, respectively, had the highest and lowest exergy destruction rates compared to other components. The results of the parametric study also showed that with the increase in the cross-section of the photovoltaic panel, the output power and cost of the electric power production increase and the exergy efficiency and the carbon dioxide emission index decrease. Asgari et al. [11] proposed a tri-generation system of power, heating, and cooling based on the gasification of biomass fuel and evaluated it from the energy and exergy perspectives. In their proposed system, urban waste and atmospheric air entered the gasifier and hot syngas were produced. The high-temperature gases from the gasification system flowed into the steam generator and produced steam, and the steam was used for heating and cooling purposes. The tri-generation system in this study was designed for the summer and winter seasons. Based on the results obtained from the system analysis, the gas turbine unit had the highest exergy destruction rate among the components of the proposed system. Also, energy efficiency, exergy efficiency, and heat and chill production rates were calculated as 71.25%, 30.796%, 40 MW, and 34.15 MW, respectively. Zoghi et al. [12] performed thermo-economic and environmental analyses of a new multi-generation system consisting of five subsystems for heat recovery of gas turbine cycle combined with solar tower and biomass gasification. In this research, gas turbine and steam Rankine subsystems were used for power generation, lithium bromide-water absorption refrigeration subsystem for cooling, proton exchange electrolyzer for hydrogen production and storage, and hot water generator for heating. The combustion products of the gas turbine cycle, after being utilized in the heat recovery heat exchanger, were used in the hot water generator and the absorption refrigeration cycle's generator, respectively. The analysis results for the case study revealed that the gas turbine cycle has an exergy efficiency of 34.7%, which increases to 43.74% by adding other subsystems. Also, in the parametric study of the proposed system, by changing the compressor pressure ratio in the gas turbine to 11.2 and 14.6, respectively, the net output power and exergy efficiency of the multi-generation system reached their maximum values. Renzi and Riolfi [13] investigated the effect of using syngas as input fuel of the combustion process in the performance of a micro gas turbine with steam injection. The obtained results showed that the thermal efficiency of the system in combustion mode with syngas can reach 75%. They also found that in the modified configuration, the exhaust gases allow for steam injection up to 65 gr/s.

Abdullah et al. [14] studied the economic analysis and optimized a power generation system based on biomass fuel. In this study, they used biogas produced by burning municipal solid waste as fuel in a gas turbine unit. Also, they proposed two separate systems in order to compare their performances from energy and economic aspects. In the first proposed system, the waste heat of the gas turbine unit was used in the recompression Brayton cycle with carbon dioxide as the working fluid to generate power. In the second proposed system, in order to improve the overall performance, a water-ammonia single-effect absorption refrigeration cycle was used to cool the carbon dioxide fluid entering the compressor. They concluded that by adding an absorption refrigeration unit for cooling the compressor's inlet fluid, the system's net output power, exergy efficiency, and unit exergy cost of products can reach, respectively, from 12080 kW to 13458 kW, from 41.28% to 45.99%, and from 7.019 $/GJ reached 6.675 $/GJ. Also, the parametric study results revealed that with the increase in the inlet temperature to the gas turbine, the net power of the system and the exergy efficiency increase and the unit exergy cost of products decreases.

As it was stated before, the construction of renewable power plants, especially the hybrid type which simultaneously utilizes solar energy, is the future and desirable trend of the power plant industry and urban management, and Therefore, in the present study, the combination of solar power plant with central receiver and the waste incinerator power plant of syngas combustion type obtained from gasification procedure is evaluated from the energy, exergy, and environmental viewpoints. In this research, the central receiver power plant consists of three main parts: heliostat, central receiver, and power block. The central receiver part, in which air is used as a heat transfer fluid, is analyzed from the energy and exergy viewpoints, and also, the effect of key operational parameters on the system performance is investigated. The amount of the total area is calculated according to the meteorological data in the city of Kerman and the intensity of solar radiation throughout the year for the central receiving power plant, and then, for the waste incineration section using the gasification method, the calorific value of the waste components was determined by collecting global standard information.

2. Nomenclature

Φ	Equivalence ratio
DNI	Direct normal irradiation
A_{helio}	Total heliostats area
N_{helio}	Total number of heliostat mirrors
$A_{single,helio}$	Single heliostat area
C	Concentration ratio of CRS
m	Air molar ratio of gasification process
$\underline{h}$	Specific enthalpy
$\overline{h}$	Specific molar enthalpy
rec	received
R_{AC}	Actual air-to-fuel ratio
d	Thickness
$\Delta T_{p.p.}$	Pinch point temperature difference
$\dot{m}$	Mass flow rate
$\dot{Q}$	Heat transfer rate
$\dot{W}$	Produced/consumed power
η_{FP}	Feed pump isentropic efficiency
η_{HPP}	High-pressure pump isentropic efficiency
$\dot{E}$	Total exergy flow
$\dot{E}_{th}$	Thermomechanical exergy flow
$\dot{E}_{ch}$	Chemical exergy flow
$\dot{I}$	Exergy destruction rate
s	Specific entropy
η_I	Energy efficiency
η_{II}	Exergy efficiency
ζ	Carbon dioxide emission index
DWH	Domestic hot water
HRSG	Heat recovery steam generator

3. System modeling

In this section, firstly, the functional principles and thermodynamic modeling of the gasification process and the solar tower along with its peripheral equipment are investigated and then the processes and components of the cogeneration system studied in this research are described along with its combination with the gasifier and the solar tower. Then, the relationships governing the components of the whole cogeneration system from the energy and exergy perspectives are expressed. Finally, the problem-solving algorithm is presented along with the flowchart of modeling the entire system.

Table 1. Final analysis results of standard urban solid waste [19] and wood [17] and their moisture percentage

Biomass type	C	H	N	S	O	Ash	HHV $\left(\frac{kJ}{kmol}\right)$	MC (%)
Municipal solid waste	47.6	6	1.2	0.3	32.9	12	433034	%16
wood	50	6	0	0	44	0	449568	%20

3.1. Gasification process modeling

In order to produce the required syngas as a combustible fuel in the external combustion chamber of the cogeneration system, municipal solid waste is used. The composition of the waste used in the gasifier is considered according to the composition presented in the references [15–18]. The mass percentage of different elements of urban solid waste, which is based on the average values of the final analyses of solid waste from different cities in the world, is stated in Table 1.

The final analysis of municipal solid waste has obtained the equivalent hydrocarbon, which produces syngas in the gasification chamber according to the following chemical reaction, and considering that the gasification reaction is carried out in adiabatic mode, the energy balance equation is according to Eq.(2) [16,17].

$$CH_{1.502}O_{0.519}N_{0.0216} + wH_2O + m[O_2 + 3.76N_2] \rightarrow aCO + bH_2 + cCO_2 + dH_2O + eN_2 + fCH_4 \quad (1)$$

$$\begin{aligned}\dot{Q}_{gassifier} = 0 \rightarrow & \left\{\bar{h}_{CH_{1.502}O_{0.519}N_{0.0216}} + w\,\bar{h}_{H2O} + m\left(\bar{h}_{O2} + 3.76\,\bar{h}_{N2}\right)\right\}|_{T=T_{ambient}} \\ = & \left\{a\,\bar{h}_{CO} + b\,\bar{h}_{H2} + c\,\bar{h}_{CO2} + d\,\bar{h}_{H2O} + e\,\bar{h}_{N2} + f\,\bar{h}_{CH4}\right\}|_{T=T_{gasification}}\end{aligned} \quad (2)$$

In the above equation, w is the molar percentage of moisture in the waste and is calculated based on Eq.(3), and m is the number of moles of air per mole of waste.

$$w = \frac{M_{fuel} \times MC}{18 \times (1 - MC)} \quad (3)$$

where at Eq.(3), M_{fuel} indicates the molecular weight of the investigated MSW where its value is 22.13 kg/kmol. and number 18 indicates the molecular weight of water which exists as humidity inside the MSW.

The chemical equilibrium for the species participating in the combustion reaction gives the following set of equations:

$$C: 1 = a + c \quad (4.a)$$

$$H: 1.502 = 2b + 2d + 4f \quad (4.b)$$

$$O: 0.5189 + w + 2m = a + 2c + d \quad (4.c)$$

$$N: 0.20162 + 2m = 2e \quad (4.d)$$

Also, the chemical balances of water-gas shifting and methane reforming among the product species are established according to the following reactions [11,16]:

$$CO_2 + H_2 \rightleftarrows CO + H_2O \quad (5.a)$$

$$CH_4 + H_2O \rightleftarrows CO + 3\,H_2 \quad (5.b)$$

The chemical equilibrium constants of the above reaction are obtained from the following equation [11,16]:

$$K_s = \exp\left(-\frac{\Delta\bar{G}_s^{\,0}}{\bar{R}T_{product}}\right) = \frac{ad}{bc} \quad (6.a)$$

$$K_R = \exp\left(-\frac{\Delta\bar{G}_R^{\,0}}{\bar{R}T_{product}}\right) = \frac{ab^3}{fd}\left(\frac{P_{gasification}}{P_0\ N_{total}}\right)^2 \quad (6.b)$$

where, $T_{product}$ is the temperature of products or gasification temperature. Also, $P_{gasification}$ is the pressure of the gasification process, which is equal to the atmospheric pressure. Also, the quantities $\Delta\bar{G}_s^{\,0}$ and $\Delta\bar{G}_R^{\,0}$ are the changes of molar Gibbs function in chemical equilibrium reactions with atmospheric pressure. In Eq.(6.b), the power of 2 indicates the difference between the stoichiometric coefficient of the products and the reactants on both sides of the equation.[16,20].

$$\Delta\bar{G}_s^{\,0} = \bar{g}^0_{CO} + \bar{g}^0_{H_2O} - \bar{g}^0_{CO_2} - \bar{g}^0_{H_2} \quad (7.a)$$

$$\Delta\bar{G}_R^{\,0} = 3\,\bar{g}^0_{CO} + \bar{g}^0_{H_2} - \bar{g}^0_{CH_4} - \bar{g}^0_{H_2O} \quad (7.b)$$

3.2. Modeling of syngas combustion chamber system

In order to make full use of syngas, the combustion reaction equation is considered as complete combustion with excess air, which is expressed in Eq. (8).

$$\dot{n}_{CO}CO + \dot{n}_{H_2}H_2 + \dot{n}_{CO_2}CO_2 + \dot{n}_{H_2O}H_2O + \dot{n}_{CH_4}\ CH_4 + \dot{n}_{N_2}\ N_2 + \frac{A_s}{\varphi}[O_2 + 3.76\ N_2] \rightarrow \dot{n}_{CO_2,\ CC}CO_2 + \dot{n}_{H_2O,CC}H_2O + \dot{n}_{O_2,CC}O_2 + \dot{n}_{N_2,CC}N_2 \quad (8)$$

Based on the law of conservation of energy and the adiabatic assumption of the combustion process in the external combustion chamber, the temperature of the combustion products is determined based on Eq. (9) [16]:

$$Q_{C.C.} = 0 \rightarrow \ \dot{n}_{CO}\ \overline{h}_{CO} + \dot{n}_{H_2}\ \overline{h}_{H_2} + \dot{n}_{CO_2}\ \overline{h}_{CO_2} + \dot{n}_{H_2O}\ \overline{h}_{H_2O} + \dot{n}_{CH_4}\ \overline{h}_{CH_4} + \dot{n}_{N_2}\ \overline{h}_{N_2} + \frac{A_s}{\varphi}\left[\ \overline{h}_{O_2} + 3.76\ \overline{h}_{N_2}\right] = \dot{n}_{CO_2,CC}\ \overline{h}_{CO_2,CC} + \dot{n}_{H_2O,CC}\ \overline{h}_{H_2O,CC} + \dot{n}_{O_2,CC}\ \overline{h}_{O_2,CC} + \dot{n}_{N_2,CC}\ \overline{h}_{N_2,CC} \quad (9)$$

3.3. Modeling of the central receiver (solar tower)

As mentioned before, the central receiver system (CRS) consists of three main components: heliostat, central receiver, and power block.

3.3.1. Heliostat field

The total solar radiation received by the heliostats field is equal to:

$$\dot{Q}_{helio} = A_h\ DNI \quad (10)$$

In the above relation, DNI is the amount of solar radiation received per area unit and A_h is the total area of the reflective surfaces (heliostats). Also, in this regard, $\dot{Q}_{helio}$ is a part of the sun's radiant energy that is reflected by heliostats. The energy and exergy balances for the heliostat field are written as the following equations, respectively:

$$\dot{Q}_{helio} = \dot{Q}_{receive} + \dot{Q}_{helio,loss} \quad (11)$$

$$\dot{E}x_{helio} = \dot{E}x_{receive} + \dot{E}x_{helio,loss} \quad (12)$$

In relation (11), $\dot{Q}_{helio,loss}$ is the heat loss of heliostats, which is caused by shading and blocking, reflectivity of mirrors, tracking errors, cleanliness of mirrors, etc. $\dot{Q}_{receive}$ is also the amount of energy delivered by the heliostats to the central receiver located at the top of the tower. Also, in Eq.(12), $\dot{E}x_{receive}$ shows the exergy delivered to the central receiver and $\dot{E}x_{helio,loss}$ shows the exergy losses. Exergy with solar energy radiation of heliostats can be expressed as follows:

$$\dot{E}x_{helio} = \dot{Q}_{helio}\left(1 - T_0/T_{sun}\right) \quad (13)$$

where, T_{sun} is the apparent temperature of the sun as an exergy source, which is considered to be 4500 K [21]. T_0 also shows the ambient temperature. Similarly, the exergy delivered to the central receiver is written as:

$$\dot{E}x_{receive} = \dot{Q}_{receive}\left(1 - T_0/T_{sun}\right) \quad (14)$$

3.3.2. Central receiver

As discussed in the previous part, the central receivers that are installed on top of the solar towers have been developed in different types. The analysis of this research is based on the cavity tube receiver. As the heat transfer fluid absorbs the energy reflected from the heliostats, it loses some of it through various mechanisms (reflection, conduction, radiation) [22]. The energy and exergy balance equations for the hollow tubular central receiver are as follows:

$$\dot{Q}_{received} = \dot{Q}_{absorb} + \dot{Q}_{loss,receiver} = \dot{m}_{air}\left(h_x - h_2\right) + \dot{Q}_{loss,receiver} \quad (15)$$

$$\dot{E}x_{received} = \dot{E}x_{absorb} + \dot{E}x_{loss,receiver} + \dot{I}_{receiver} \quad (16)$$

In the above equations, $\dot{Q}_{absorb}$ and $\dot{E}x_{absorb}$,respectively, show the amount of net radiation absorbed by the central receiver and the net exergy received in the central receiver. $\dot{Q}_{loss,receiver}$ and $\dot{E}x_{loss,receiver}$ are, respectively, the amount of total energy loss and the amount of exergy loss in the central receiver. Exergy loss is expressed along with total heat loss:

$$\dot{E}x_{loss,receive} = \dot{Q}_{rec,totloss}\left(1 - T_0/T_{rec,sur}\right) \quad (17)$$

at the above equation, $T_{rec,sur}$ indicates the surface temperature of the receiver at the solar tower which will be calculated by solving the following relations. The net exergy absorbed in the central receiver is also:

$$\dot{E}x_{absorb} = \dot{m}_{air}\left((h_x - h_2) - T_0(s_x - s_2)\right) = \dot{m}_{air}cp_{air}\left(T_x - T_2 - T_0\ln\left(T_x/T_2\right)\right) \quad (18)$$

The total heat loss in the central receiver can also be obtained by different mechanisms including radiation, reflection, and conduction [22].

$$\dot{Q}_{loss,receive} = \dot{Q}_{rec,conv+} + \dot{Q}_{rec,em} + \dot{Q}_{rec,ref} + \dot{Q}_{rec,con} \quad (19)$$

$$\dot{Q}_{rec,em} = \varepsilon_{avg}\sigma\left(T_{rec,sur}^4 - T_0^4\right) A_h / C \quad (20)$$

where C is defined as the concentration ratio as $C=A_h / A_{ape}$.

The area required for central receiving power plants is one of the important factors for designing this type of power plant. Accordingly, Ong et al. [23], used the information of several central receiving power plants to obtain the required area of these types of solar power plants to produce 1MW of electricity. According to their report, the total area is the amount of area occupied by the entire site of the central receiving power plant, and the direct area is the area occupied by solar collectors and other related facilities. The direct area for central receiving power plants, according to Ong et al., ranges from 2.1 to 5.3 acres/GWh/yr with a median value of 2.8 acres/GWh/yr. In Table 2, the amount of area required for the central receiving power plant is given according to the report of Ong et al.

Table 2. The amount of area required for the central receiving power plant [23]

Central receiving power plant	The number of projects reviewed	Capacity (MW)	Required area (acres/MW)	Area required to produce 1GWh per year
total area	14	2358	10	3.2
Direct area	9	1358	8.9	2.8

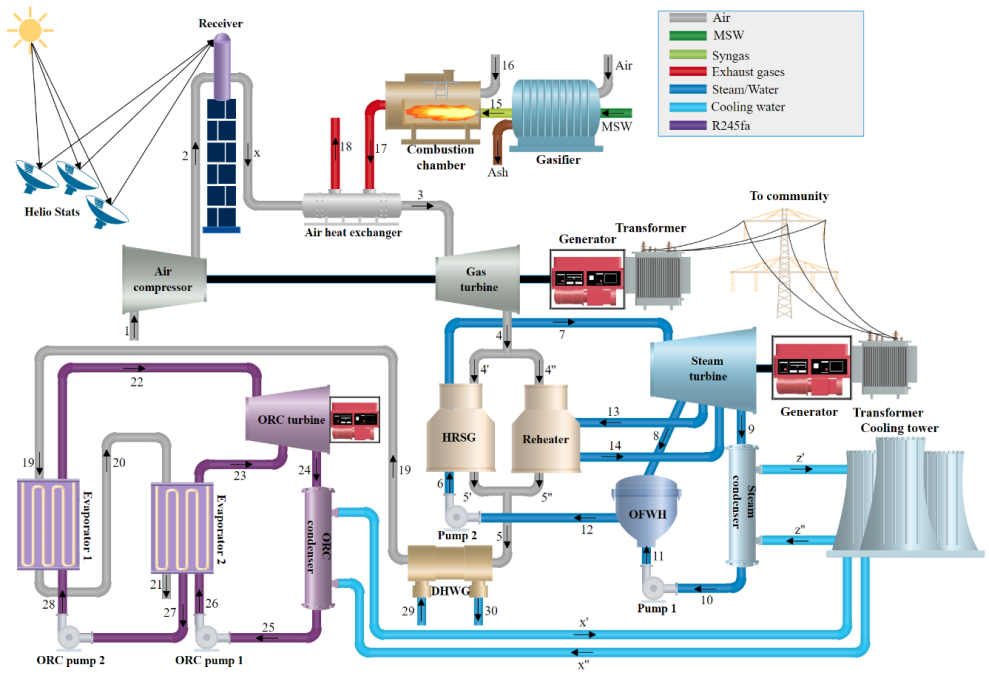

Fig. 1. Thermodynamic schematic of the proposed cogeneration system

According to the research of Ong et al. [23], it is found that to produce 1 GWh/yr of electric power based on the solar tower power plant, about 2.9 acres, that is, 0.0117363 square kilometers of space will be needed.

3.4. Cogeneration system description

The schematic of the cogeneration system proposed in the current research is shown in Fig. 1.

The cogeneration system investigated in this research consists of five subsystems, including gas turbine, steam Rankine with regenerator and reheater, and organic Rankine. In the gas turbine subsystem, air enters the compressor from point 1 in ambient conditions and compresses at a certain pressure ratio. Then, in order to receive heat, it moves towards the solar receiver, and due to the absorption of the sun's energy, its temperature increases. In order to receive more heat and reach the inlet temperature of the gas turbine, this working fluid moves towards the air heater and increases the temperature by receiving heat from the combustion products of the outlet of the chamber. In the next step, this fluid flows in the turbine and produces electric power by exchanging energy and reducing pressure. Due to the high temperature of the gas turbine output, air energy can be used for heat recovery in other subsystems. Fluid flow 4 is divided into two streams in order to produce water vapor in the Rankine subsystem. Each of the divided streams exchanges heat with the opposite fluid (water) in the heat recovery steam generators and leaves it. The outgoing air streams, being directed to the heat exchanger supplying domestic hot water, transfer another part of their energy in it, and in the final stage, they are directed to the first and second evaporators of the organic Rankine subsystem. since the outlet temperature from the HRSG is low, we have utilized ORC which is compatible with the low-temperature heat source. The organic Rankine subsystem uses two evaporators that are connected in series to heat its working fluid, and the working fluid R245fa is considered for this subsystem. The hot air stream enters the first evaporator from point 19 and transfers its heat to the organic fluid. Then, in the low-temperature evaporator, the airflow is discharged to the atmosphere by transferring the final part of the heat, and the organic fluid leaves the second evaporator after receiving heat. condenser inlet temperature of ORC and Rankine Cycle are 25^{O}C and the condenser outlet temperature which moves towards the dry cooling tower is assumed to be 35^{O}C.

3.5. Thermodynamic modeling of the cogeneration system

In this section, the basic assumptions are stated in order to model the cogeneration system. In the following, the relationships governing the components are explained from the first and second laws of thermodynamics points of view.

3.5.1. Assumptions

In the thermodynamic analysis of the investigated cogeneration system, the following initial assumptions have been used:

1. The components of the cogeneration system work in steady state.
2. The effects of changing the kinetic energy and the potential of the working fluid flows can be ignored.
3. The pressure loss in the pipes connecting the components can be neglected.
4. The gases in the cogeneration system follow the ideal gas behavior.
5. Heat exchangers are properly insulated and therefore, heat transfer to the outside environment is ignored.
6. The combustion and gasification chamber are adiabatic and their heat transfers to the outside environment are omitted.
7. The values of pressure and ambient temperature to determine the flow exergies of the operating fluids of each of the subsystems are considered to be 101.3 kPa and 25°C, respectively.

3.5.2. Energy analysis relations

In order to balance the energy of the components of the cogeneration system, the first law of thermodynamics is used. Also, the mass or molar flow rates of different flows of working fluids are determined using the law of conservation of mass.

$$\sum_{\text{inlets}} \dot{m}_i = \sum_{\text{outlets}} \dot{m}_e \tag{21}$$

$$\dot{Q}_{cv} - \dot{W}_{cv} = \sum_{inlets} \dot{m}_i h_i - \sum_{outlets} \dot{m}_e h_e \quad (22)$$

In these equations, indices i are used for inputs and indices e are used for outputs of volume controls. According to Fig. 1, for the equipment used in each of the subsystems, the relationships of the energy conservation law are given in Table 3.

3.5.3. Exergy analysis relations

The exergy balance relationship for the control volume that works in steady state is as follows:

$$\sum_{inlets} \dot{E}_i + \Sigma \dot{Q}_j \left(1 - \frac{T_0}{T_j}\right) = \sum_{outlets} \dot{E}_e + \dot{W}_{cv} + \dot{I}_{cv} \quad (23)$$

The total flow exergy of the working fluid, $\dot{E}$, is equal to the sum of the thermomechanical and chemical flow exergies.

$$\dot{E} = \dot{E}_{th} + \dot{E}_{ch} \quad (24)$$

Thermomechanical flow exergy for the working fluid is determined using the following equation:

$$\dot{E}_{th} = \sum \dot{m}_i \left[(h_i - h_0) - T_0 (s_i - s_0) \right] \quad (25)$$

Chemical flow exergy is also obtained for a mixture of ideal gases using the following equation:

$$\dot{E}_{ch} = n(\sum y_i \bar{e}_i^{ch.0} + \bar{R} T_0 \sum y_i \ln(y_i) \quad (26)$$

The chemical exergy of hydrocarbons equivalent to municipal solid waste (biomass) can be calculated based on its constituent elements as the following Eq. (27) [24]:

$$\dot{E}_{ch,fuel} = \beta \, LHV_{MSW} \quad (27)$$

where LHV_{MSW} is equal to the low calorific value of waste, which is obtained from the final analysis of municipal solid waste in Table1. Also, the quantity β is (reference given):

$$\beta = \frac{1.044 + 0.16 \times \left(\frac{H_{mass}}{C_{mass}}\right) - 0.34493 \times \left(\frac{O_{mass}}{C_{mass}}\right) \times \left(1 + 0.0531 \times \left(\frac{H_{mass}}{C_{mass}}\right)\right)}{1 - 0.4142 \times \frac{O_{mass}}{C_{mass}}} \quad (28)$$

Table 3. Energy balance relations of components of the cogeneration system

Gas turbine subsystem	
Component	**Energy balance equation**
Air compressor	$\dot{h}_1 + \dot{W}_{comp} = \dot{h}_2$
Gasifier	$\dot{h}_{MSW} + \dot{h}_{Air} = \dot{h}_{15}$
Combustion chamber	$\dot{h}_{15} + \dot{h}_{16} = \dot{h}_{17}$
Heat exchanger	$\dot{h}_x + \dot{h}_{17} = \dot{h}_3 + \dot{h}_{18}$
Gas turbine	$\dot{h}_4 + \dot{W}_{Turb} = \dot{h}_3$
Organic Rankine subsystem with working fluid R245fa	
Component	Energy balance equation
Pump 1	$\dot{h}_{25} + \dot{W}_{ORC,P1} = \dot{h}_{26}$
Pump 2	$\dot{h}_{27} + \dot{W}_{ORC,P2} = \dot{h}_{28}$
Evaporator 1	$\dot{h}_{19} + \dot{h}_{28} = \dot{h}_{20} + \dot{h}_{22}$
Evaporator 2	$\dot{h}_{20} + \dot{h}_{26} = \dot{H}_{23} + \dot{h}_{21}$
ORC turbine	$\dot{h}_{24} + \dot{W}_{ORC,Turb} = \dot{h}_{23} + \dot{h}_{22}$
ORC condenser	$\dot{h}_{24} + \dot{h}_{x}'' = \dot{h}_{25} + \dot{h}_{x}'$
Hot water generator subsystem	
Component	Energy balance equation
Heat exchanger producing hot water	$\dot{h}_5 + \dot{h}_{29} = \dot{h}_{19} + \dot{h}_{30}$
Steam Rankine subsystem	
Component	Energy balance equation
Heat recovery steam generator	$\dot{h}_{4}' + \dot{h}_6 = \dot{h}_{5}' + \dot{h}_7$
Open feed water heater	$\dot{h}_{4}'' + \dot{h}_{13} = \dot{h}_{5}'' + \dot{h}_{14}$
Steam turbine	$\dot{h}_8 + \dot{h}_9 + \dot{h}_{13} + \dot{W}_{Steam,Turb} = \dot{h}_7 + \dot{h}_{14}$
Pump 1	$\dot{h}_{10} + \dot{W}_{Steam,P1} = \dot{h}_{11}$
Pump 2	$\dot{h}_{12} + \dot{W}_{Steam,P1} = \dot{h}_6$
Steam condenser	$\dot{h}_9 + \dot{h}_{z}'' = \dot{h}_{10} + \dot{h}_{z}'$
Open feed water heater	$\dot{h}_8 + \dot{h}_{11} = \dot{h}_{12}$
Cooling tower	$\dot{h}_{x}' + \dot{h}_{z}' = \dot{h}_{x}'' + \dot{h}_{z}''$

Table 4. Exergy balance relations of components of the power generation system

Gas turbine subsystem	
Component	**Exergy balance equation**
Air compressor	$\dot{E}_1 + \dot{W}_{comp} = \dot{E}_2 + \dot{I}_{comp}$
Gasification	$\dot{E}_{MSW} + \dot{E}_{Air} = \dot{E}_{15} + \dot{I}_{Gasifier}$
Combustion chamber	$\dot{E}_{15} + \dot{E}_{16} = \dot{E}_{17} + \dot{I}_{cc}$
Heat exchanger	$\dot{E}_x + \dot{E}_{17} = \dot{E}_3 + \dot{E}_{18} + \dot{I}_{cc}$
Gas turbine	$\dot{E}_4 + \dot{W}_{Turb} + \dot{I}_{Turb} = \dot{E}_3$
Organic Rankine subsystem with working fluid R245fa	
Component	Exergy balance equation
Pump 1	$\dot{E}_{25} + \dot{W}_{ORC,P1} = \dot{E}_{26} + \dot{I}_{ORC,P1}$
Pump 2	$\dot{E}_{27} + \dot{W}_{ORC,P2} = \dot{E}_{28} + \dot{I}_{ORC,P2}$
Evaporator 1	$\dot{E}_{19} + \dot{E}_{28} = \dot{E}_{20} + \dot{E}_{22} + \dot{I}_{Evap1}$
Evaporator 2	$\dot{E}_{20} + \dot{E}_{26} = \dot{E}_{23} + \dot{E}_{21} + \dot{I}_{Evap2}$
ORC turbine	$\dot{E}_{24} + \dot{W}_{ORC,Turb} + \dot{I}_{ORC,Turb} = \dot{E}_{23} + \dot{E}_{22}$
ORC condenser	$\dot{E}_{24} + \dot{E}_{x}'' = \dot{E}_{25} + \dot{E}_{x}' + \dot{I}_{Cond}$
Hot water generator subsystem	
Component	Exergy balance equation
Heat exchanger producing hot water	$\dot{E}_5 + \dot{E}_{29} = \dot{E}_{19} + \dot{E}_{30} + \dot{I}_{DHWG}$
Steam Rankine subsystem	
Component	Exergy balance equation
Heat recovery steam generator	$\dot{E}_4' + E_6 = \dot{E}_5' + \dot{E}_7 + \dot{I}_{HRSG}$
Open heater	$\dot{E}_4'' + \dot{E}_{13} = \dot{E}_5'' + \dot{E}_{14} + \dot{I}_{Reheat}$
Steam turbine	$\dot{E}_8 + \dot{E}_9 + \dot{E}_{13} + \dot{W}_{Steam,Turb} + \dot{I}_{Steam,Turb} = \dot{E}_7 + \dot{E}_{14}$
Pump 1	$\dot{E}_{10} + \dot{W}_{Steam,P1} = \dot{E}_{11} + \dot{I}_{Steam,P1}$
Pump 2	$\dot{E}_{12} + \dot{W}_{Steam,P1} = \dot{E}_6 + \dot{I}_{Steam,P2}$
Steam condenser	$\dot{E}_9 + E_z'' = \dot{E}_{10} + \dot{E}_z' + \dot{I}_{Steam,Cond}$
Open feed water heater	$\dot{E}_8 + \dot{E}_{11} = \dot{E}_{12} + \dot{I}_{OFWH}$
Cooling tower	$\dot{E}_x' + \dot{E}_z' = \dot{E}_x'' + E_z'' + \dot{I}_{Cooling}$

According to Fig. 1, for the equipment used in each of the subsystems, the exergy balance relations are given in Table 4.

2.6. Energy efficiency, exergy efficiency, and carbon dioxide emission index

The efficiency of the first law for subsystems of gas turbine, steam Rankine, organic Rankine, and also, the efficiency of the whole system are respectively [3,25,26]:

$$\eta_{Isteam} = \frac{\dot{W}_{net,steam}}{\dot{Q}_{HRSG} + \dot{Q}_{REHEAT}} \quad (29)$$

$$\eta_{Iair} = \frac{\dot{W}_{net,air}}{\dot{Q}_{tot,in}} \quad (30)$$

$$\eta_{IORC} = \frac{\dot{W}_{net,ORC}}{\dot{H}_{19} - \dot{H}_{21}} \quad (31)$$

$$\eta_{I,total} = \frac{\dot{W}_{net,total} + \dot{H}_{30} - \dot{H}_{29}}{DNI\ A_{helio} + \dot{m}_{MSW}\ LHV_{MSW}} \quad (32)$$

where at Eq.(30), $Q_{tot,in}$ indicates the total received thermal power from both the solar tower and the syngas combustion chamber.

For each subsystem of the combined of power and heat plant, as well as the whole system, exergy efficiency as a measure to express the quality of the energy used is defined as follows [3,25,26]:

$$\eta_{II,steam} = \frac{\dot{W}_{net,steam}}{\dot{E}x_7 - \dot{E}x_6 + \dot{E}x_{14} - \dot{E}x_{13}} \quad (33)$$

$$\eta_{II,air} = \frac{\dot{W}_{net,air}}{\dot{E}x_3 - \dot{E}x_2} \quad (34)$$

$$\eta_{II,ORC} = \frac{\dot{W}_{net,ORC}}{\dot{E}x_{19} - \dot{E}x_{21}} \quad (35)$$

$$\eta_{II,total} = \frac{\dot{W}_{net,tot} + \dot{E}x_{30} - \dot{E}x_{29}}{\dot{E}x_{helio} + \dot{E}x_{MSW}} \quad (36)$$

The carbon dioxide emission index of the entire cogeneration system is:

$$\xi = \frac{\dot{m}_{CO_2,p}}{\dot{W}_{net}} \times 3600 \quad (37)$$

2.7. Problem-solving algorithm and properties of the basic system of the central receiving part

The thermodynamic modeling flowchart of the cogeneration system is shown in Fig. 2.

The properties of the basic system of the central receiving part in the solar tower part of the power plant are shown in Table 5.

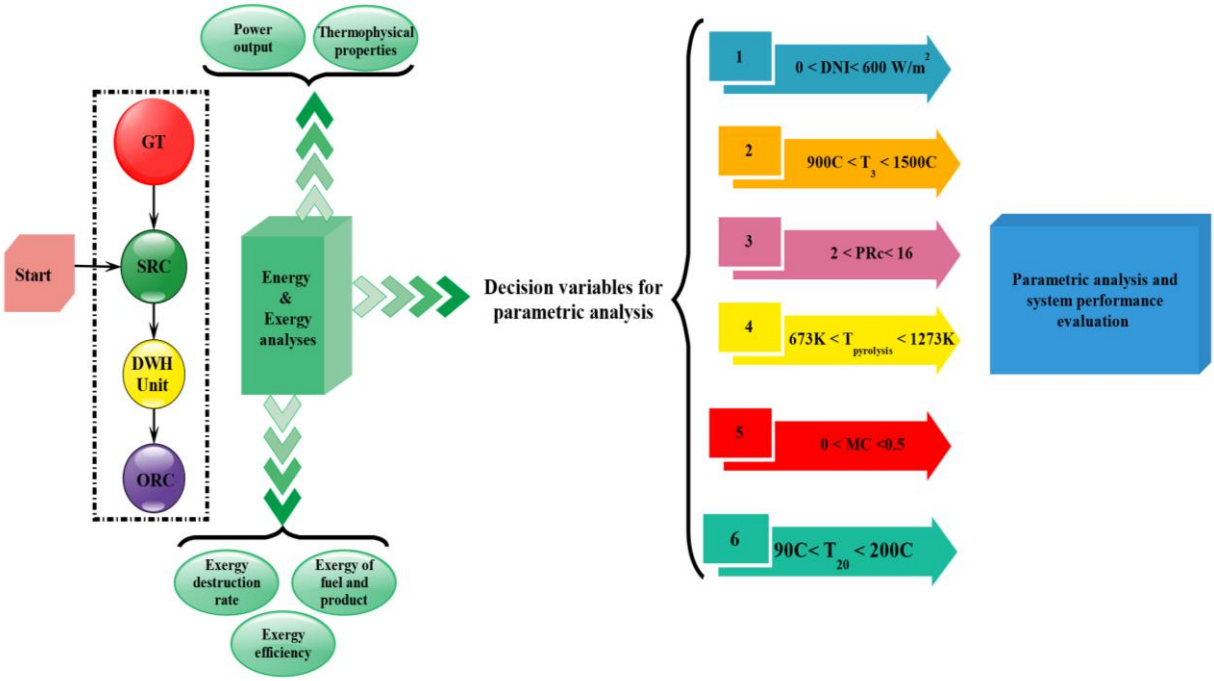

Fig. 2. Flowchart of thermodynamic modeling of the cogeneration system

Table 5. Properties of the base system of the central receiving power plant [3]

Subsystem	Properties	Values	Unit
Heliostat field	Beam radiation (DNI)	600	$W.m^{-2}$
	Apparent Sun Temperature	4500	K
	Overall field efficiency	90%	–
	A heliostat mirror area	14.05	m^2
	Number of mirrors	2500	–
	Total heliostat area	35125	m^2
Central receiver	Aperture area	12.5	m^2
	Overall receiver efficiency	90%	–
	Inlet temperature of Air	321.9	℃
	Outlet temperature of Air	1000	℃
	Concentration ratio	2810	–

3. Results and discussion

3.1. Validation of gasification process

In order to verify and ensure the performance of the gasification process, the molar percentages of the products of the gasification process obtained from the modeling of the present work are compared with reference [15] and experimental results [16,17]. Based on the molar balance and taking into account the chemical equilibrium conditions of the products, the molar percentages of the output syngas have been compared with the results obtained from references [15–17] in Table 6. According to the table, it can be seen that the obtained results are in good agreement with the references.

3.2. Model of activity and control of solar hybrid power plant-combustion of syngas

According to the hybrid nature of the power plant studied in this research, the system is generally divided into three working modes:

1. Fully solar activity (the heat source of the system is only solar energy.)
2. Fully combustion activity (the heat source of the system is only the combustion of syngas resulting from gasification)
3. Hybrid activity with two active heat sources (both the sun and the syngas combustion system are active at the same time.)

In this way, as the average solar radiation start time approaches, the amount of waste consumed is reduced and the required energy is provided from solar radiation, and When the average solar radiation start time is reached, the waste pyrolysis section is completely deactivated. After the time of full solar activity of the system, in the last hours of the day, the process of switching between sources, once again in the opposite direction; That is, the decrease in the use of the sun and the increase in the share of the waste pyrolysis sector continue until sunset and at the end of the switching period, the power and heat production system is fully fed by the combustion heat source of syngas obtained from the waste pyrolysis.

In order to create stability and uniform production of power through the heat source of the sun, we are satisfied with the daily average power. With this method, in addition to the fact that the production becomes uniform and fixed for several hours (for about 5-7 hours), the effects of the prevailing weather are also controlled to some extent. For example, when the weather is partly cloudy, it is possible to reach the average value of radiation, which will not affect the produced power. The advantage of this method is clearly shown in Fig. 3, which shows the instantaneous intensity index of direct solar radiation on the 14th of April 2012 at the synoptic station of Rafsanjan city. As can be seen, at certain hours of the day, the DNI index faces many ups and downs due to atmospheric changes and clouds, which can be eliminated by using the daily average method.

3.3. Case study of power and heat production system

Basic information and input parameters in the case study of power and heat production system are given in Table 7.

Considering the assumptions stated in the previous section and the thermodynamic relations governing the components of the power and heat production system, the modeling of the cogeneration system was done and the analysis results are given in Table 8.

The efficiency values of the first and second laws of the power and heat production system as well as the carbon dioxide emission index for all three working modes of fully solar activity, fully syngas combustion activity, and hybrid activity at DNI=0.45 are given in Table 9.

Grossman diagrams of exergy flows and processes performed in the cogeneration system for three working modes of the hybrid power plant are shown in Figs. 4, respectively.

Table 6. Validation of molar percentages obtained from wood gasification process with references [15–17]

Species	Current study	Reference [15]	Reference [16]	Reference [17]
H_2	17.98	17.15	15.50	18.04
CO	18.66	19.28	19.10	17.86
CH_4	0.0024	0.55	1.10	0.11
CO_2	12.38	10.81	11.40	11.84
N_2	50.99	52.21	52.90	52.15

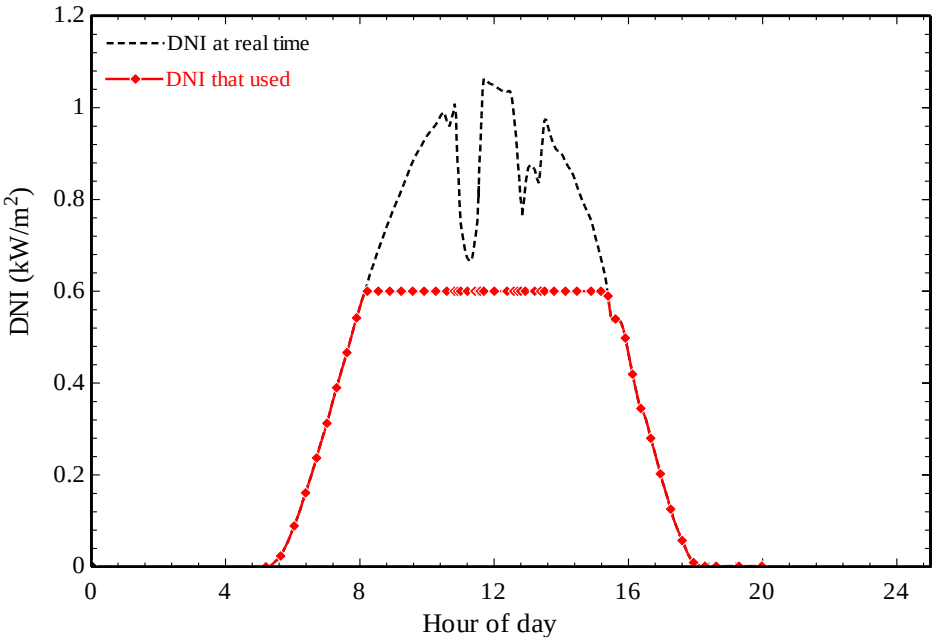

Fig. 3. The trends of instant DNI and average DNI

Table 7. Basic input data for the study of the cogeneration system

Input parameter	Indication	Value	Unit	Reference
Ambient pressure	P_0	101.3	kPa	[27]
Environment temperature	T_0	25	℃	[27]
Combustion chamber equivalence ratio	Φ	0.9	-	[27]
Air compressor pressure ratio	PR	8	-	[28]
Intensity of vertical solar radiation	DNI	600	W/m^2	[29]
The working pressure of the gasification process	$P_{gasification}$	101.3	kPa	[15]
Lateral area of the central receiver	$A_{aperture}$	12.5	m^2	[3]
Area of each solar mirror	$A_{heliostat}$	14.05	m^2	[3]
Central receiver efficiency	$\eta_{receiver}$	0.90	-	[28]
Solar mirror efficiency	$\eta_{heliostat}$	0.90	-	[28]
Air compressor efficiency	η_{comp}	0.80	-	[28]
Gas turbine efficiency	$\eta_{air,turb}$	0.85	-	[28]
Efficiency of Rankine cycle pumps	$\eta_{p,st}$	0.90	-	[3]
Efficiency of high pressure and low-pressure Rankine steam turbines	$\eta_{st,turb}$	0.85	-	[3]
Organic Rankine cycle turbine efficiency	$\eta_{ORC,turb}$	0.75	-	[30]
Efficiency of organic Rankine cycle pumps	$\eta_{ORC,p}$	0.60	-	[30]
Functional temperature of the gasification process	$T_{gasification}$	1100	K	[15]
Gas turbine inlet temperature	T_3	1000	℃	[28]
Pinch point temperature difference of steam Rankine heat exchangers	$\Delta T_{PP,ST}$	5	℃	[28]
Pinch point temperature difference of organic Rankine heat exchangers	$\Delta T_{PP,ORC}$	5	℃	[30]
Working temperature of high-pressure organic Rankine evaporator	$T_{eva1,ORC}$	77	℃	[30]
Low-pressure organic Rankine evaporator working temperature	$T_{eva2,ORC}$	70	℃	[30]

Table 8. Thermodynamic properties of operating fluids at different points of the power and heat production system

State	Pressure [kPa]	Temperature [C]	Mass flow rate [kg/s]	Enthalpy [KJ/Kg]	Entropy [KJ/Kg. K]	Chemical exergy [kW]	Total exergy [kW]
1	101.3	25	22.4	298.6	5.696	-	0
2	810.4	321.9	22.4	602.1	5.803	-	6082
3	810.4	1000	22.4	1364	6.651	-	17490
4	101.3	560.9	22.4	859.8	6.763	-	5439
5	101.3	284.4	22.4	562.9	6.332	-	1672
6	12600	239	2.373	1034	2.673	-	573.2
7	12600	550	2.373	3475	6.627	-	3569
8	3150	352.9	0.6701	3120	6.729	-	749.1
9	10	45.81	1.703	2546	8.03	-	266.3
10	10	45.81	1.703	191.8	0.6492	-	4.782
11	3150	45.99	1.703	195.3	0.6503	-	10.22
12	3150	236.6	2.373	1021	2.67	-	544.7
13	2520	326.4	0.6701	3072	6.749	-	1812
14	2520	550	0.6701	3574	7.461	-	2306
15	101.3	826.9	2.441	2256	9.019	6162	7509
16	101.3	25	1.829	0	6.736	8.144	8.144
17	101.3	1632	4.27	-1290	8.996	422.7	6381
18	101.3	917	4.27	-2289	8.34	422.7	2948
19	101.3	120	22.4	394.3	5.975	-	283.3
20	101.3	79.62	22.4	353.6	5.865	-	99.89
21	101.3	6045	22.4	334.2	5.809	-	43.19
22	732.7	82	5.348	465.6	1.794	-	196.8
23	609.7	75	0.6282	460.7	1.79	-	2083
24	177.2	48.82	5.976	444.7	1.812	-	63.5
25	177.2	30	5.976	239.1	1.135	-	40.38
26	609.7	3032	5.976	239.7	1.136	-	37.9
27	609.7	70	5.348	294.6	1.306	-	6065
28	732.7	70.12	5.348	294.8	1.306	-	61.25
29	101.3	25	25.8	104.9	0.3672	-	0
30	101.3	60	25.8	251.2	0.8312	-	205.7

Table 9. Energy efficiency and exergy of power and heat production system

Activity mode	Carbon dioxide emission index $\left[\frac{kg}{kWh}\right]$	Exergy efficiency%	Energy efficiency%
Hybrid	0.4966	29.54	44.3
Fully solar	0	37.94	52.36
Fully combustible	1.248	28.24	48.23

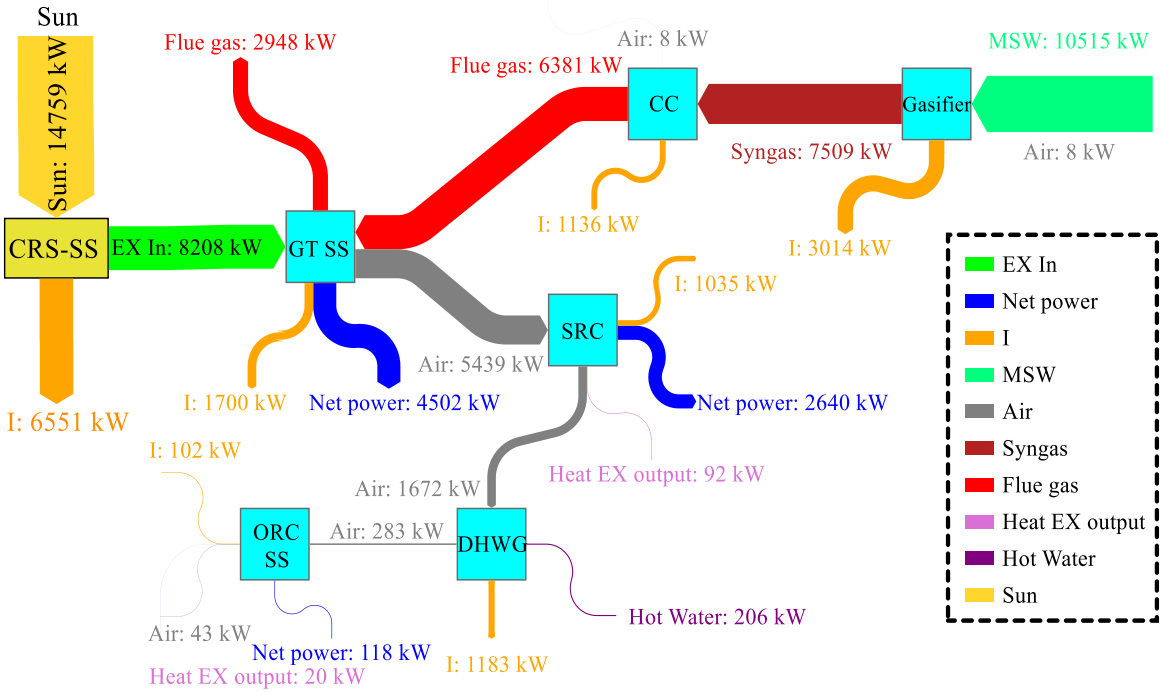

Fig. 4a. Grossman diagram of exergy flows of the cogeneration system processes in the hybrid mode for DNI=0.45

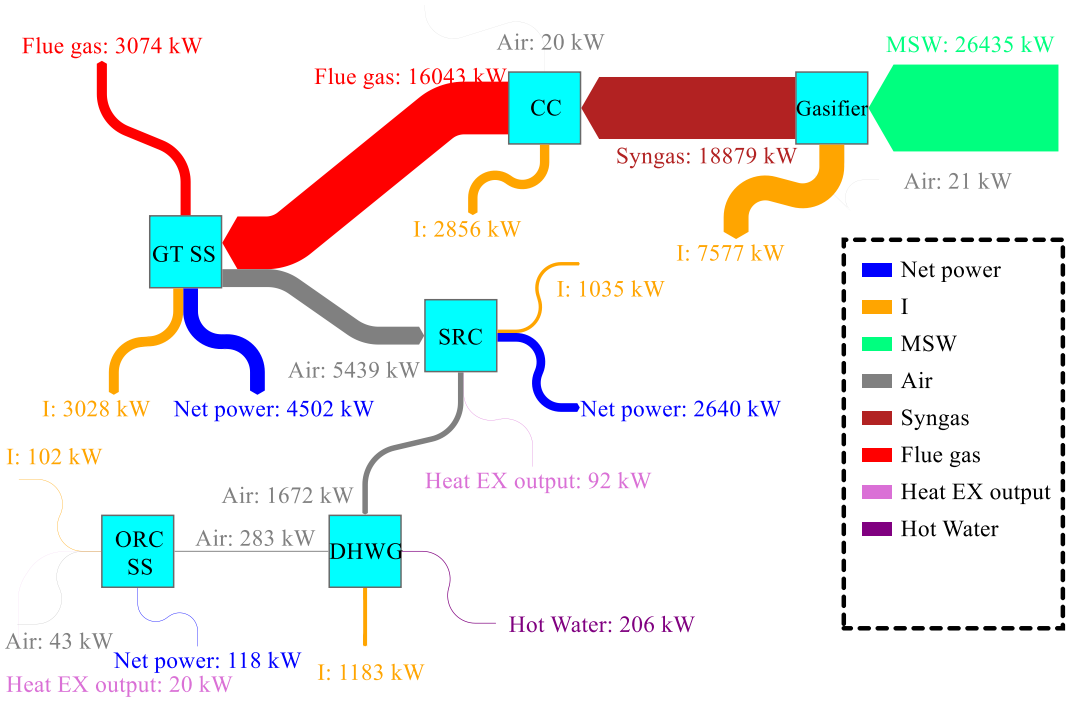

Fig. 4b. Grossman diagram of exergy flows of the cogeneration system processes in fully combustion mode for DNI=0

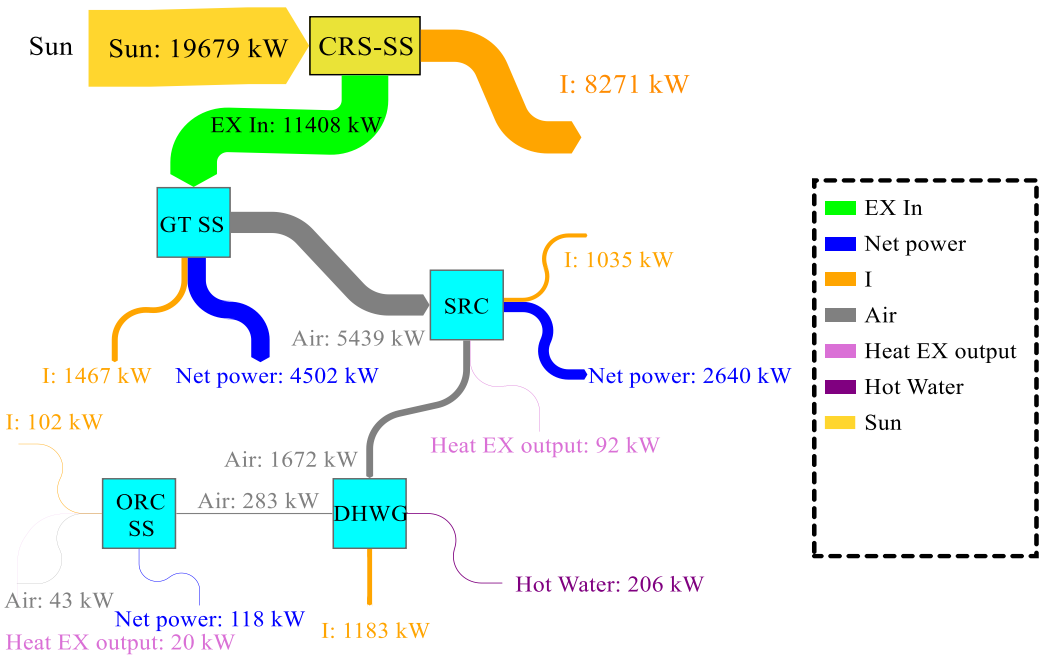

Fig. 4c. Grossman diagram of exergy flows of the cogeneration system processes in fully solar mode for DNI=0.6

In Fig. 5, the pie charts of the percentage of exergy destruction of each of the constituent components of the cogeneration subsystems are shown.

The bar-circle diagram of the power production of each of the cogeneration subsystems is shown in Fig. 6.

3.4. Parametric study of the cogeneration system

In order to investigate the performance of the cogeneration system based on gas turbine, a parametric study was conducted on the key variables and the obtained results are presented in the form of diagrams.

3.4.1. Studying the effect of compressor pressure ratio on the performance of the system

According to Fig. 7a, with the increase in air compressor pressure ratio, the net production power of the system first increases and then decreases. As the pressure ratio increases, the gas turbine outlet temperature decreases and as a result, the production power of the gas turbine subsystem and organic Rankine cycle continuously increase, but the production power of the steam Rankine subsystem decreases. This dual behavior causes the trend of the net production power of the entire system to be upward and then downward.

According to the diagram in Fig. 7b, with the increase in the pressure ratio of the air compressor, the efficiency of the whole system always increases from the value of 29.1% to 44.33%.

According to the diagram in Fig. 7c, it can be seen that for the production of constant power of 6MW, the consumption flow rate of waste is always increasing with a gentle slope compared to the increase in the compressor pressure ratio, which is due to the increase in air flow rate due to the decrease in the temperature difference of the terminals of the heat exchanger.

According to Fig. 7d, as the compressor pressure ratio increases, the carbon dioxide emission index first decreases and then increases.

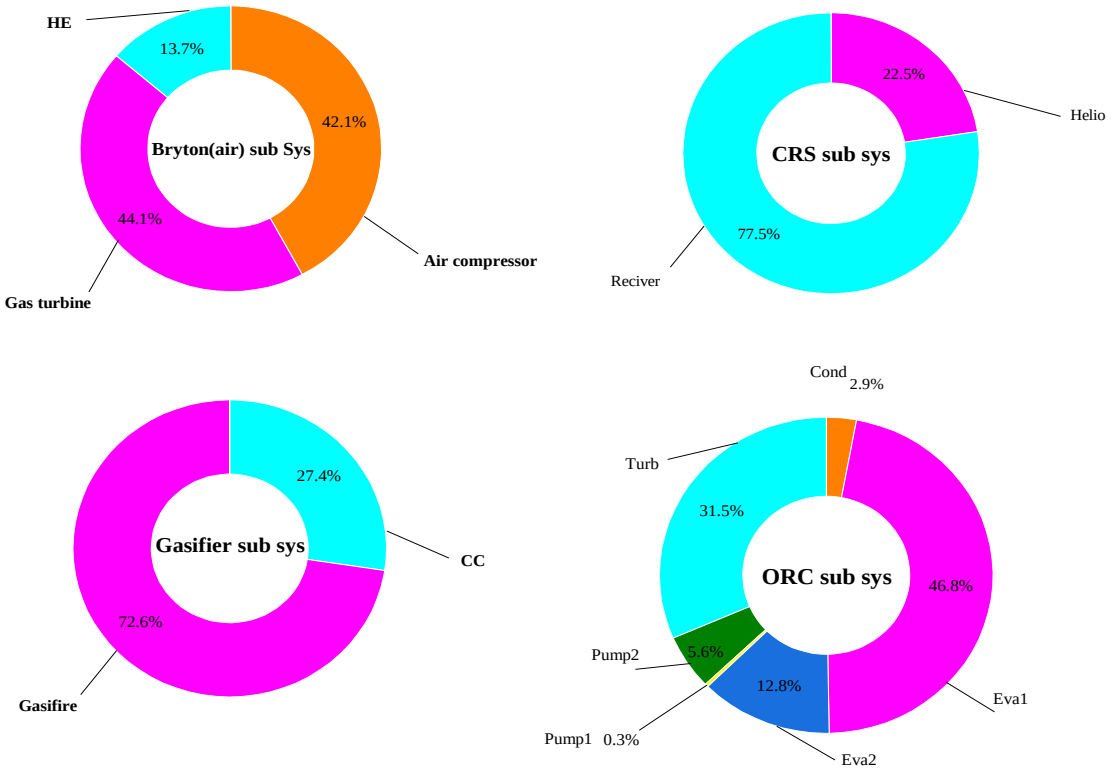

Fig. 5. Pie charts of percentage of exergy destruction of each component of the cogeneration subsystems

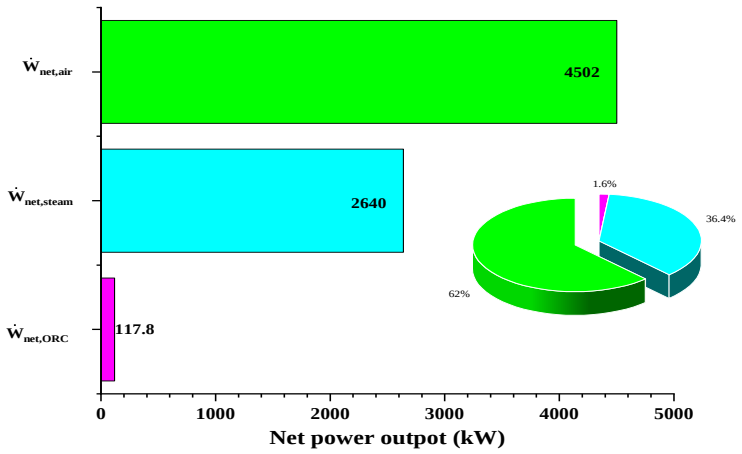

Fig. 6. bar-circle diagram of each subsystem of the combined heat and power plant

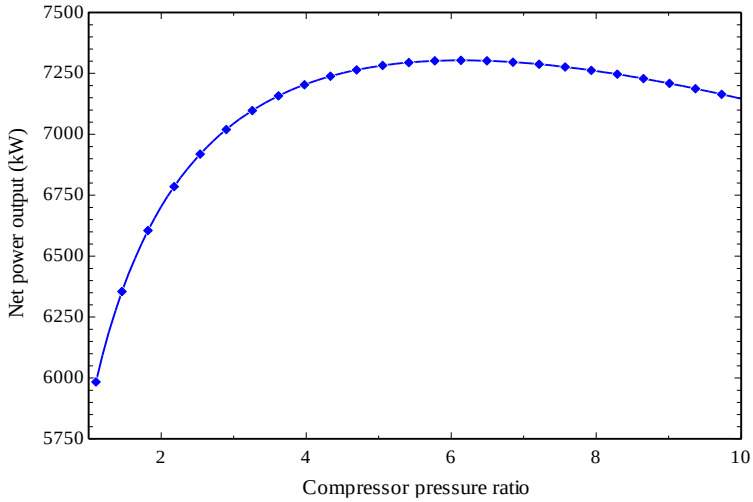

Fig. 7a. The graph of the net power of the entire cogeneration system against the pressure ratio of the air compressor

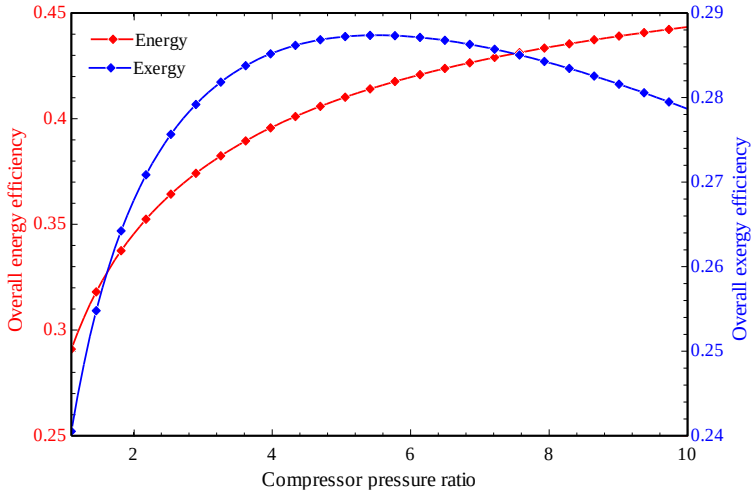

Fig. 7b. Diagram of energy and exergy efficiencies of the cogeneration system against the pressure ratio of the air compressor

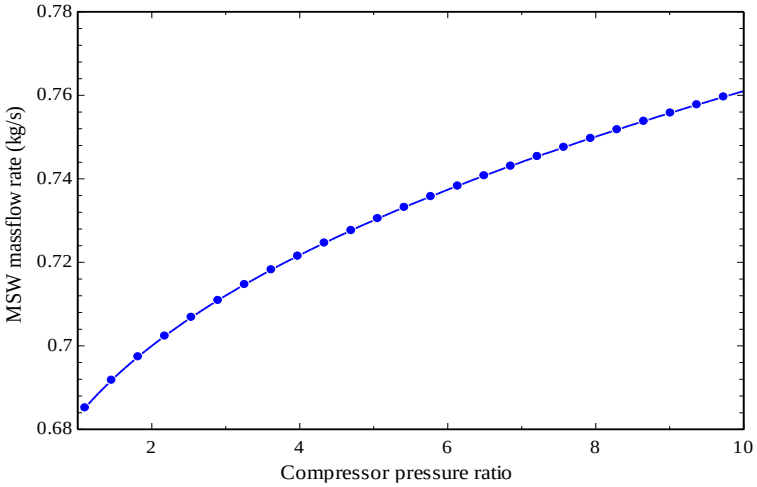

Fig. 7c. Graph of waste consumption flow versus compressor pressure ratio

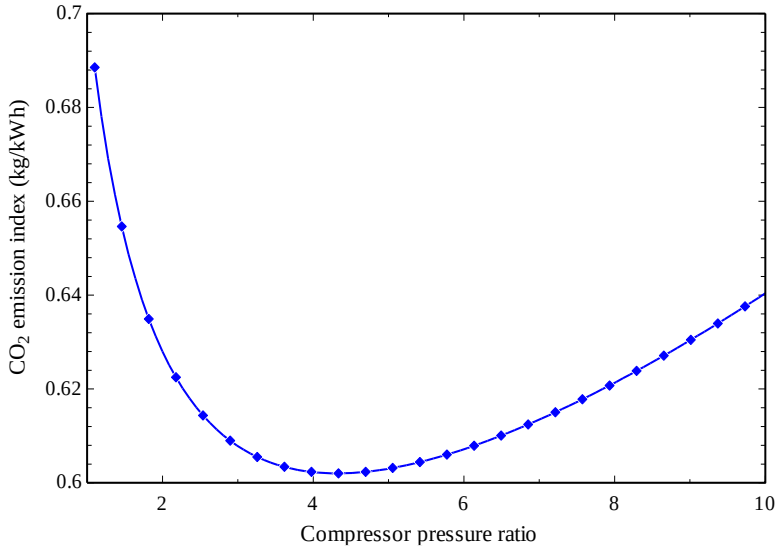

Fig. 7d. The effect of compressor pressure ratio on carbon dioxide emission index

3.4.2. The effect of the temperature of the gasification process on the performance of the system

By changing the temperature of the gasification process, the molar percentage of syngas species resulting from the gasification and pyrolysis process changes according to Fig. 8a. It can be seen that with the increase in temperature, the concentration of produced methane decreases and the concentration of hydrogen and carbon monoxide in syngas increases. dry syngas consists of the molar ratio of three combustible gases (Hydrogen, Carbon monoxide and Methane) against all the gasification products except water (H2O).

According to the diagram in Fig. 8b, with the increase in the temperature of the gasification process, the flow of consumed waste is associated with a slight decrease. According to the figure, it can be seen that with the increase in the temperature of the gasification process, the consumption flow rate of waste is decreasing.

As the gasification temperature increases, the amount of air used, i.e., the ratio of air to fuel required in the gasification process, will increase as shown in Fig. 8c.

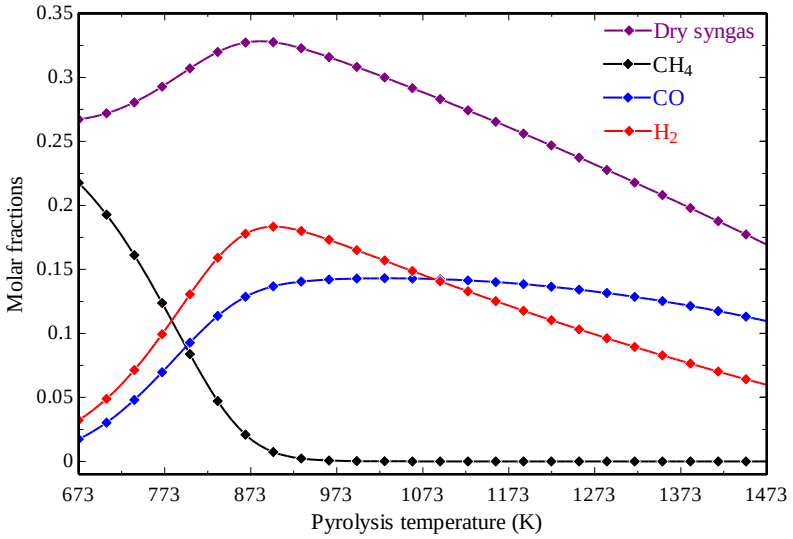

Fig. 8a. Diagram of the influence of the temperature of the gasification process on the molar percentage of syngas species

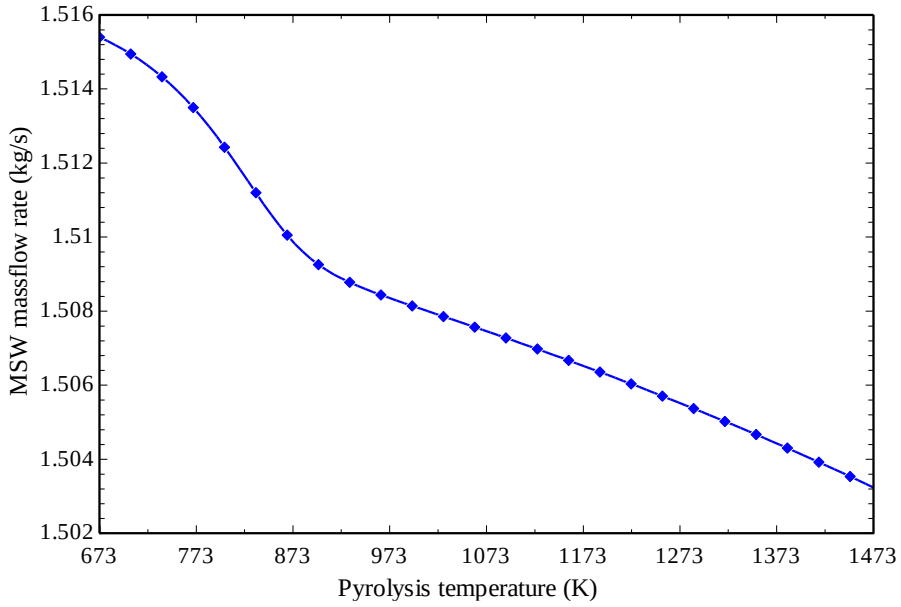

Fig. 8b. The effect of the temperature of the gasification process on the consumption flow of waste

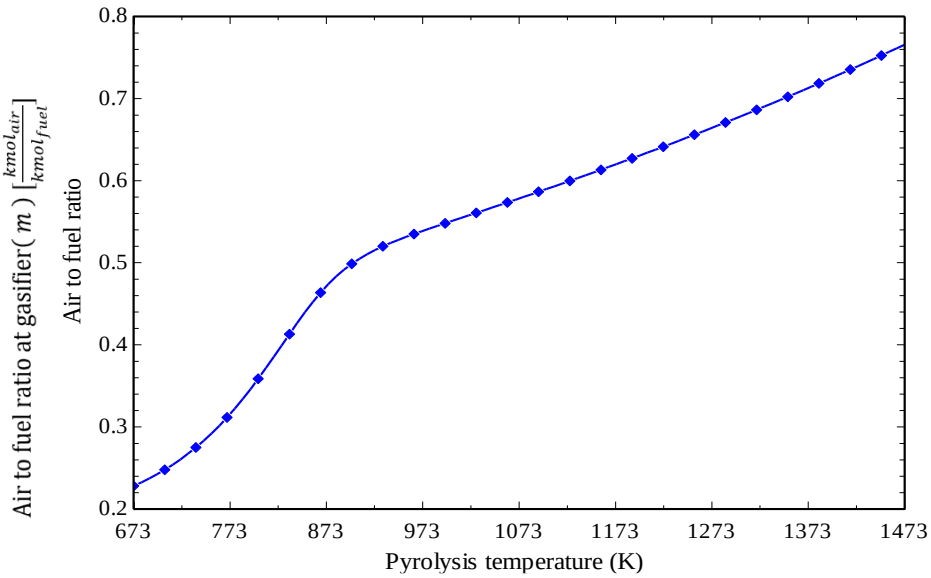

Fig. 8c. The effect of gasification process temperature on the ratio of air to fuel in this process

In Fig. 8d, the graph of energy efficiency and exergy of the entire system is shown against the temperature of the gasification process. According to this diagram, the total energy and exergy efficiencies increase with the increase in the temperature of the gasification process. Since the temperature of the gasification chamber is derived from the half-burnt MSW, in order to increase the gasification reactor temperature, more air inflow is required so that the gasification reaction gets closer to the combustion.

In Fig. 8e, the graph of the carbon dioxide emission index of the cogeneration system against the temperature of the gasification process is shown. According to this diagram, the carbon dioxide emission index decreases as the temperature of the gasification process increases.

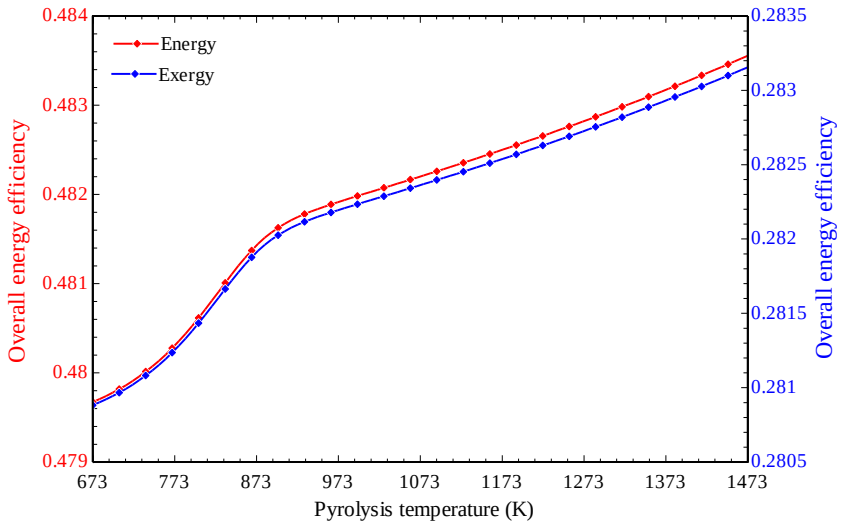

Fig. 8d. The effect of the temperature of the gasification process on the energy and exergy efficiencies

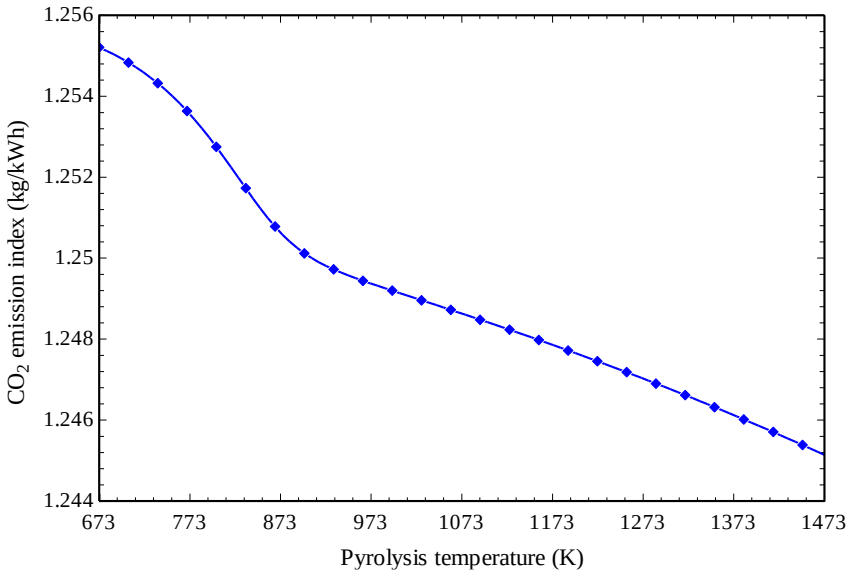

Fig. 8e. The effect of the temperature of the gasification process on the carbon dioxide emission index

3.4.3. The effect of gas turbine inlet temperature on the performance of the system

By increasing the inlet temperature of the gas turbine according to Fig. 9a, the production power of the entire system will increase as follows. The reason for this process is the higher effect of temperature increase on the increase of production power against the lower effect of reducing the flow rate of air entering the turbine. As the inlet temperature increases, due to the decrease in the airflow rate in the Brighton cycle, the heat is exchanged in the urban hot water heater and as a result, the urban hot water flow rate decreases.

According to the diagram in Fig. 9b, the increase in the inlet temperature to the gas turbine will decrease the efficiency of the entire system despite the increase of the total production power, which is due to the decrease in the flow rate of urban hot water production, which is directly effective on the efficiency of the first law of the entire system.

According to Fig. 9c, it can be seen that with the increase in the inlet temperature of the gas turbine, due to the decrease in the airflow rate, the urban hot water flow rate decreases from 33.39 to 7.3 kg/s.

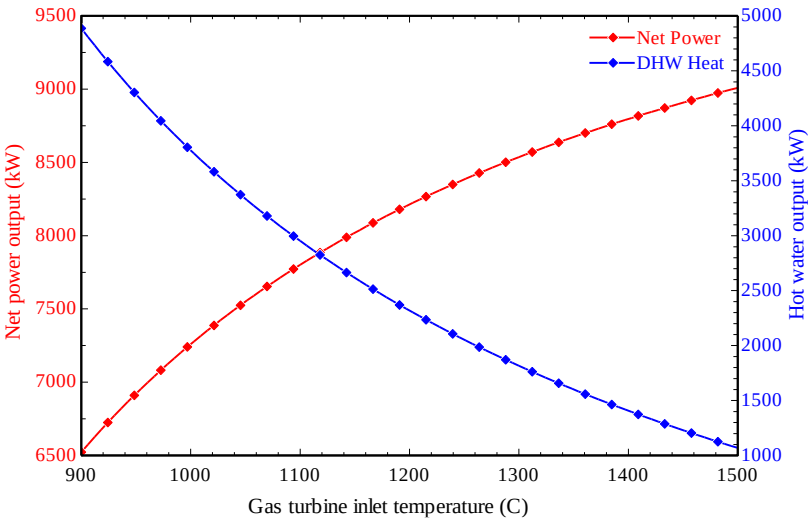

Fig. 9a. The influence of the gas turbine inlet temperature on the total production of power and urban hot water heat

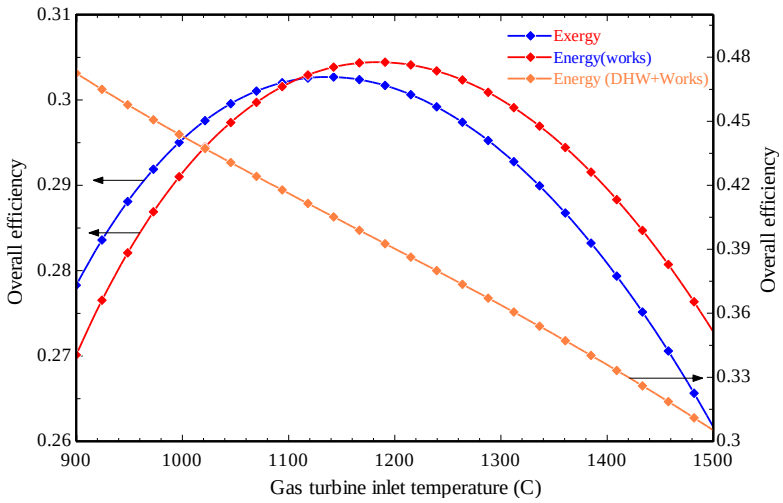

Fig. 9b. The effect of gas turbine inlet temperature on the overall efficiency of the system

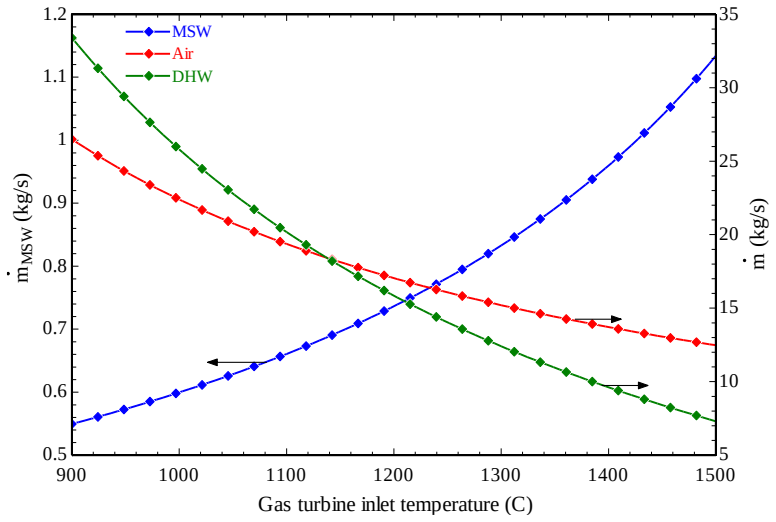

Fig. 9c. The influence of the gas turbine inlet temperature on the urban hot water generation

Figure 9d shows the effect of the gas turbine inlet temperature on the carbon dioxide emission index. According to the figure, as the gas turbine inlet temperature increases, the carbon dioxide emission index increases. This increment is due to the increase of the MSW mass flow rate at the gasification reactor and because of the increase in the mass flow rate of the burned syngas inside the combustion chamber.

According to Fig. 10a, with the increase of radiation intensity in the early morning to noon; That is, from DNI equal to 0 to 0.3, the efficiency of the first law of the whole system faces a drop, which is caused by the heat of the solar system entering the denominator of the relation of the overall efficiency of the first law. If the mass flow rate of waste does not decrease significantly, this will reduce the effect of the heat value of the input to the system in the denominator of the relationship. But after the passage of time, the value of DNI from the value of 0.3 with a more noticeable reduction in the consumption of waste, its reducing effect in the share of the denominator is also greater, and since the magnitude of the share of solar energy is smaller than the heat value of the waste through the waste, as a result, the denominator is smaller. Also, the exergy efficiency of the whole system can be expressed with the same reasoning, the first downward and then increasing trend of the exergy efficiency of the whole system can be expressed. In general, it is concluded that the system in transition and switching mode has a much lower efficiency than the stable mode of solar only (6 hours of day) and waste only mode (12 hours of night) and in general, the operation of the system in solar mode has a higher efficiency than the garbage incinerator mode.

According to Fig. 10b, the consumption waste flow for the total constant power decreases at the beginning with a slower process, which effect was discussed in the overall efficiency of the system, and at the end, it decreases at a much faster rate. According to this behavior, it seems that the gas system is better to work at its full capacity than at half capacity.

In Fig. 10c, it can be seen that due to the increase of direct solar radiation (DNI), and keeping the total heat input to the system and the output power of the system constant, the contribution of each of the heat sources will be determined as follows. As can be seen, with the increase of DNI, the share of the sun decreases, and the share of the gasifier increases.

According to Fig. 10d, it can be seen that due to the expected decrease in the share of the gasification sector in the production of power, the production of carbon dioxide will also decrease; But according to the previous studies, firstly, this reduction is due to the slower reduction of the waste flow and the carbon dioxide flow will also decrease slowly; But at the end, this reduction becomes faster and finally, with the completion of the sun's share in the production of carbon dioxide production power, it reaches zero, which is considered to be environmentally clean production.

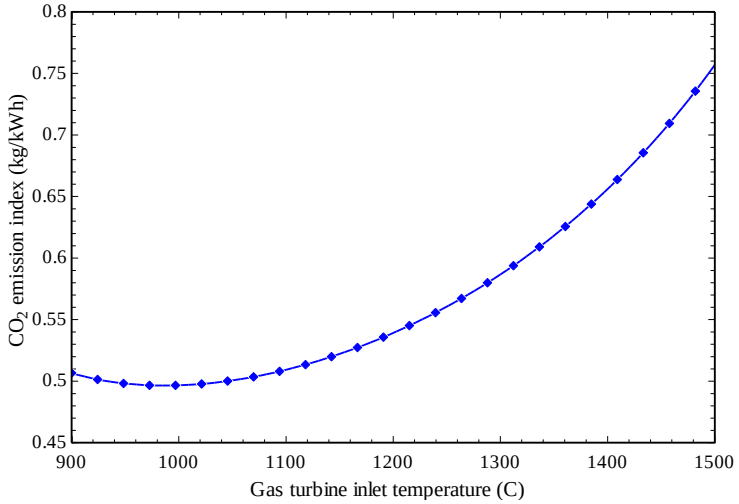

Fig. 9d. The effect of gas turbine inlet temperature on carbon dioxide emission index

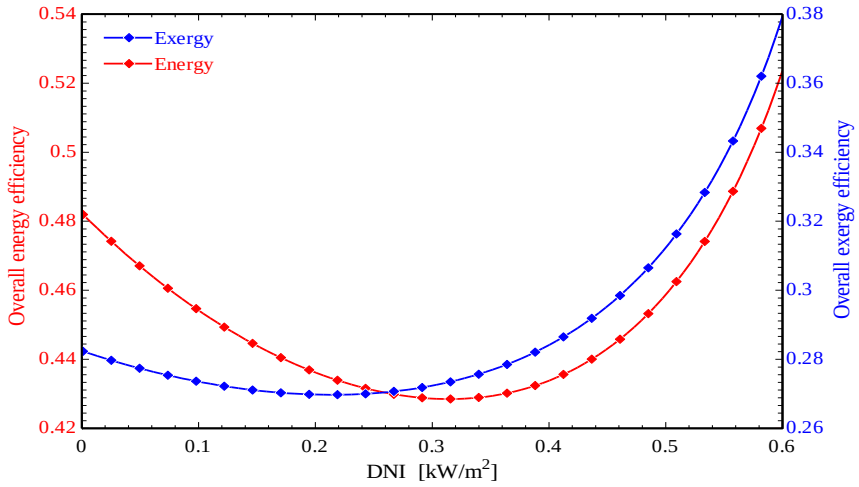

Fig. 10a. The effect of solar radiation intensity on the overall efficiency of the system

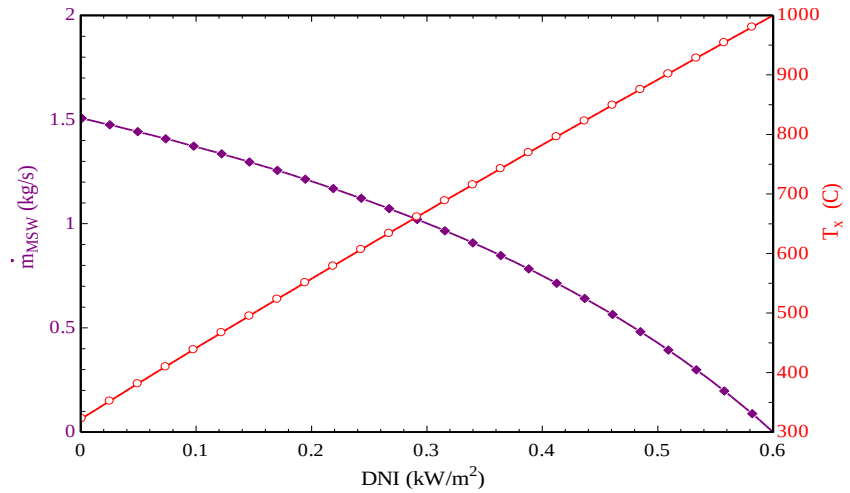

Fig. 10b. The effect of solar radiation intensity on the flow of waste consumed in the gasification system

3.4.4. The effect of solar radiation intensity on the performance of the system

According to Figure 10a, with the increase of radiation intensity in the early morning to noon; That is, from DNI equal to 0 to 0.3, the efficiency of the first law of the whole system faces a drop, which is caused by the heat of the solar system entering the denominator of the relation of the overall efficiency of the first law. If the mass flow rate of waste does not decrease significantly, this will reduce the effect of the heat value of the input to the system in the denominator of the relationship. But after the passage of time, the value of DNI from the value of 0.3 with a more noticeable reduction in the consumption of waste, its reducing effect in the share of the denominator is also greater, and since the magnitude of the share of solar energy is smaller than the heat value of the waste through the waste, as a result, the denominator is smaller. Also, the exergy efficiency of the whole system can be expressed with the same reasoning, the first downward and then increasing trend of the exergy efficiency of the whole system can be expressed. In general, it is concluded that the system in transition and switching mode has a much lower efficiency than the stable mode of solar only (6 hours of day) and waste only mode (12 hours of night) and in general, the operation of the system in solar mode has a higher efficiency than the garbage incinerator mode.

According to Fig.10b, the consumption waste flow for the total constant power decreases at the beginning with a slower process, which effect was discussed in the overall efficiency of the system, and at the end, it decreases at a much faster rate. According to this behavior, it seems that the gas system is better to work at its full capacity than at half capacity.

In Fig.10c, it can be seen that due to the increase of direct solar radiation (DNI), and keeping the total heat input to the system and the output power of the system constant, the contribution of each of the heat sources will be determined as follows. As can be seen, with the increase of DNI, the share of the sun decreases and the share of the gasifier increases.

According to Fig,10d, it can be seen that due to the expected decrease in the share of the gasification sector in the production of power, the production of carbon dioxide will also decrease; But according to the previous studies, firstly, this reduction is due to the slower reduction of the waste flow and the carbon dioxide flow will also decrease slowly; But at the end, this reduction becomes faster and finally, with the completion of the sun's share in the production of carbon dioxide production power, it reaches zero, which is considered to be environmentally clean production.

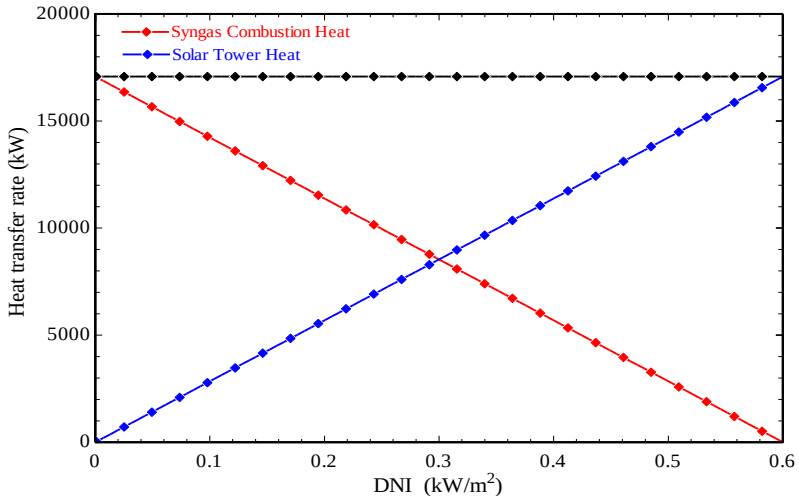

Fig. 10c. The effect of solar radiation intensity on the changes in the thermal contribution of both gasifier and solar tower thermal subsystems

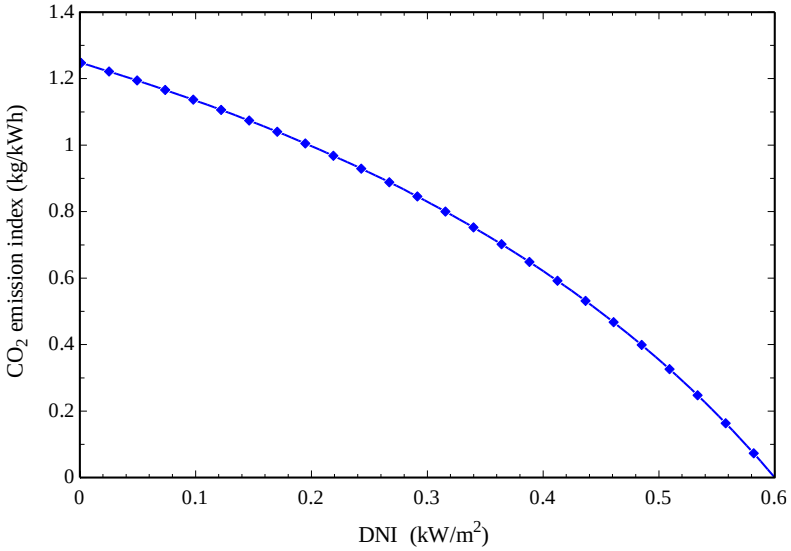

Fig. 10d. The effect of solar radiation intensity on carbon dioxide greenhouse gas emissions

3.4.5. Overview of the contribution of effective heat sources in the system in 24 hours a day based on the average daily DNI

Figure 11 shows the activity and contribution of each of the heat sources used in the cogeneration system against DNI and considers the daily average DNI. According to this graph, which is for the 14th day of April 2013, the importance of using the average DNI method is evident. Therefore, from 0:00 midnight to 5:00 a.m., the power plant works fully using the gasifier and waste system, and after this hour, with the sunrise, the share of the sun increases, and as a result, until 8:00 a.m. In the morning, it reaches its full capacity, when the waste incinerator section is completely turned off according to the figure, and the production continues using only the solar source until 15.5 in the afternoon, and after that, with the reduction of solar radiation, the waste incinerator system is activated and the power production system works with two sources.

5. Conclusions

In the present study, thermodynamic analysis of a hybrid solar-biomass cogeneration system was performed from the perspectives of energy and exergy. This power plant included the subsystems of the central receiver of the solar tower and the syngas combustion system obtained from the gasification of urban solid waste, Brayton air cycle with external combustion, Rankine steam cycle, organic Rankine cycle, and domestic hot water generator. The hot air coming out of the gas turbine served as the heat source of the steam Rankine and organic Rankine cycles and the hot water generator. The results obtained from the thermodynamic analysis of the system indicate that according to the amount of solar radiation in the current research area, 6 hours of work as solar tower only, 6 hours of work as pyrolysis, and 6 hours of combined work are required. The results obtained from the case study of the cogeneration system revealed that the electrical powers produced by the subsystems of the air Brayton cycle, the reheat Rankine cycle and the organic Rankine cycle are equal to 4502.6 KW, 2640.3 KW and 118 KW, respectively. The mass flow rate of hot water supplied from the thermal recovery generator subsystem was calculated as 25.8 kg/s. The central receiver of the solar tower had the highest rate of irreversibility, accounting for 34% of the total exergy destruction rate. The results of the parametric. study also showed that the total net power produced first increases and then decreases with the increase in the Brayton cycle's inlet air temperature. Also, the irreversibility of the entire system was directly related to the increase in the inlet temperature of the turbine.

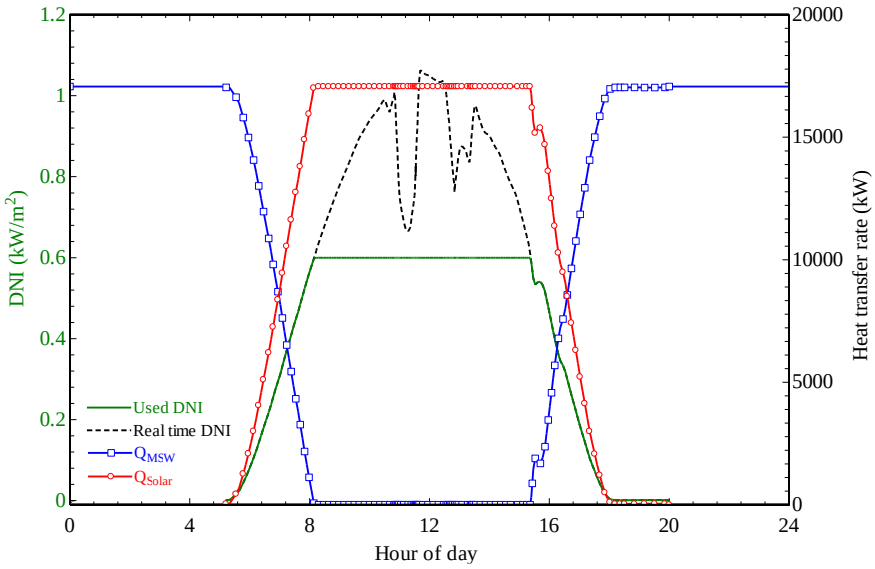

Fig. 11. Changes in solar thermal sources and waste incinerator of the overall system during the hours of day and night based on the average daily radiation intensity method

Investigating the effect of the percentage of moisture in the waste consumed in the gasification sector on the performance variables showed that the increase of this moisture leads to a decrease in the temperature and percentage of syngas produced and finally, it causes a decrease in the performance of the system. The net power of the entire system increased first and then decreased with the increase in the temperature of the gasification process and, as a result, the increase in the temperature of the incoming gases to the external heat exchanger of the Brayton cycle.

References

[1] Datta A, Ganguly R, Sarkar L. Energy and exergy analyses of an externally fired gas turbine (EFGT) cycle integrated with biomass gasifier for distributed power generation. Energy 2010;35:341–50. https://doi.org/https://doi.org/10.1016/j.energy.2009.09.031.

[2] Noghani F, Noghanibehambari H. Product Market Competition, Corporate Governance, And Managerial Slack: Evidence from Trade Liberalization. J Leadership, Account Ethics 2019;16. https://doi.org/10.33423/jlae.v16i4.2372.

[3] Xu C, Wang Z, Li X, Sun F. Energy and exergy analysis of solar power tower plants. Appl Therm Eng 2011;31:3904–13. https://doi.org/https://doi.org/10.1016/j.applthermaleng.2011.07.038.

[4] Siva Reddy V, Kaushik SC, Ranjan KR, Tyagi SK. State-of-the-art of solar thermal power plants—A review. Renew Sustain Energy Rev 2013;27:258–73. https://doi.org/https://doi.org/10.1016/j.rser.2013.06.037.

[5] Miller FJ, Koenigsdorff RW. Thermal Modeling of a Small-Particle Solar Central Receiver . J Sol Energy Eng 2000;122:23–9. https://doi.org/10.1115/1.556277.

[6] Behar O, Khellaf A, Mohammedi K. A review of studies on central receiver solar thermal power plants. Renew Sustain Energy Rev 2013;23:12–39. https://doi.org/https://doi.org/10.1016/j.rser.2013.02.017.

[7] Coelho B, Varga S, Oliveira A, Mendes A. Optimization of an atmospheric air volumetric central receiver system: Impact of solar multiple, storage capacity and control strategy. Renew Energy 2014;63:392–401. https://doi.org/https://doi.org/10.1016/j.renene.2013.09.026.

[8] Tukenmez N, Yilmaz F, Ozturk M. Parametric analysis of a solar energy based multigeneration plant with SOFC for hydrogen generation. Int J Hydrogen Energy 2022;47:3266–83. https://doi.org/https://doi.org/10.1016/j.ijhydene.2021.01.131.

[9] Dunham MT, Iverson BD. High-efficiency thermodynamic power cycles for concentrated solar power systems. Renew Sustain Energy Rev 2014;30:758–70. https://doi.org/https://doi.org/10.1016/j.rser.2013.11.010.

[10] Cen S, Li K, Liu Q, Jiang Y. Solar energy-based hydrogen production and post-firing in a biomass fueled gas turbine for power generation enhancement and carbon dioxide emission reduction. Energy Convers Manag 2021;233:113941. https://doi.org/https://doi.org/10.1016/j.enconman.2021.113941.

[11] Asgari N, Khoshbakhti Saray R, Mirmasoumi S. Energy and exergy analyses of a novel seasonal CCHP system driven by a gas turbine integrated with a biomass gasification unit and a LiBr-water absorption chiller. Energy Convers Manag 2020;220:113096. https://doi.org/https://doi.org/10.1016/j.enconman.2020.113096.

[12] Zoghi M, Habibi H, Yousefi Choubari A, Ehyaei MA. Exergoeconomic and environmental analyses of a novel multi-generation system including five subsystems for efficient waste heat recovery of a regenerative gas turbine cycle with hybridization of solar power tower and biomass gasifier. Energy Convers Manag 2021;228:113702. https://doi.org/https://doi.org/10.1016/j.enconman.2020.113702.

[13] Renzi M, Riolfi C, Baratieri M. Influence of the Syngas Feed on the Combustion Process and Performance of a Micro Gas Turbine with Steam Injection. Energy Procedia 2017;105:1665–70.

https://doi.org/https://doi.org/10.1016/j.egypro.2017.03.543.

[14] Al-Rashed AAAA, Afrand M. Multi-criteria exergoeconomic optimization for a combined gas turbine-supercritical CO2 plant with compressor intake cooling fueled by biogas from anaerobic digestion. Energy 2021;223:119997. https://doi.org/https://doi.org/10.1016/j.energy.2021.119997.

[15] Jarungthammachote S, Dutta A. Thermodynamic equilibrium model and second law analysis of a downdraft waste gasifier. Energy 2007;32:1660–9. https://doi.org/https://doi.org/10.1016/j.energy.2007.01.010.

[16] Yari M, Mehr AS, Mahmoudi SMS, Santarelli M. A comparative study of two SOFC based cogeneration systems fed by municipal solid waste by means of either the gasifier or digester. Energy 2016;114:586–602. https://doi.org/https://doi.org/10.1016/j.energy.2016.08.035.

[17] Zainal ZA, Ali R, Lean CH, Seetharamu KN. Prediction of performance of a downdraft gasifier using equilibrium modeling for different biomass materials. Energy Convers Manag 2001;42:1499–515. https://doi.org/https://doi.org/10.1016/S0196-8904(00)00078-9.

[18] Gholamian E, Mahmoudi SMS, Zare V. Proposal, exergy analysis and optimization of a new biomass-based cogeneration system. Appl Therm Eng 2016;93:223–35. https://doi.org/https://doi.org/10.1016/j.applthermaleng.2015.09.095.

[19] Khan MN, Luna IZ, Islam MM, Sharmeen S, Salem KS, Rashid TU, et al. Chapter 21 - Cellulase in Waste Management Applications. In: Gupta VKBT-N and FD in MB and B, editor., Amsterdam: Elsevier; 2016, p. 237–56. https://doi.org/https://doi.org/10.1016/B978-0-444-63507-5.00021-6.

[20] Javaherian A, Yari M, Gholamian E, Carton JG, Mehr AS. Proposal and comprehensive analysis of power and green hydrogen production using a novel integration of flame-assisted fuel cell system and Vanadium-Chlorine cycle: An application of multi-objective optimization. Energy Convers Manag 2023;277:116659. https://doi.org/https://doi.org/10.1016/j.enconman.2023.116659.

[21] Sadeghi M, Chitsaz A, Marivani P, Yari M, Mahmoudi SMS. Effects of thermophysical and thermochemical recuperation on the performance of combined gas turbine and organic rankine cycle power generation system: Thermoeconomic comparison and multi-objective optimization. Energy 2020;210:118551. https://doi.org/https://doi.org/10.1016/j.energy.2020.118551.

[22] Li X, Kong W, Wang Z, Chang C, Bai F. Thermal model and thermodynamic performance of molten salt cavity receiver. Renew Energy 2010;35:981–8. https://doi.org/https://doi.org/10.1016/j.renene.2009.11.017.

[23] Ong S, Campbell C, Denholm P, Margolis R, Heath G. Land-Use Requirements for Solar Power Plants in the United States. United States: 2013. https://doi.org/10.2172/1086349.

[24] Wu Y, Yang W, Blasiak W. Energy and Exergy Analysis of High Temperature Agent Gasification of Biomass. Energies 2014;7:2107–22. https://doi.org/10.3390/en7042107.

[25] Shatnawi H, Lim CW, Ismail FB. Solar Thermal Power: Appraisal of Solar Power Towers. MATEC Web Conf 2018;225.

[26] Sonntag RE, Borgnakke C, Van Wylen GJ. Fundamentals of Thermodynamics. Wiley; 2002.

[27] Moran MJ, Shapiro HN, Boettner DD, Bailey MB. Fundamentals of Engineering Thermodynamics. Wiley; 2010.

[28] Alshahrani S, Engeda A. Performance Analysis of a Solar–Biogas Hybrid Micro Gas Turbine for Power Generation. J Sol Energy Eng 2020;143. https://doi.org/10.1115/1.4048157.

[29] The moment Prediction Global solar radiation in rafsanjan city with neural network. Iran J Energy 2014;16:15.

[30] Li T, Zhang Z, Lu J, Yang J, Hu Y. Two-stage evaporation strategy to improve system performance for organic Rankine cycle. Appl Energy 2015;150:323–34. https://doi.org/https://doi.org/10.1016/j.apenergy.2015.04.016.